JJMIE

Volume 15, Number 4, October. 2021
ISSN 1995-6665
Pages 357 - 376

Jordan Journal of Mechanical and Industrial Engineering

Numerical Study of Fluid Dynamics and Heat Transfer Characteristics for the Flow Past a Heated Square Cylinder

Rashid Ali[*,a] , Anshumaan Singh [b]

[a]*Associate Professor, Dept. of Mechanical Engg., Zakir Husain College of Engg. & Tech., Aligarh Muslim University, Aligarh Pin 202002, INDIA,*

[b]*Research Scholar, Dept. of Mechanical Engg., Zakir Husain College of Engg. & Tech., Aligarh Muslim University, Aligarh Pin 202002, INDIA*

Received November 5 2020 *Accepted September 17 2021*

Abstract

Effects of inertia and buoyancy forces are numerically investigated on fluid dynamics and heat transfer characteristics for the flow past a heated square cylinder in an unconfined flow regime. Non-dimensional number in the study chosen are Re = 1 - 45, Ri = 0 - 1.50, α = 0o– 90o. The orientation of the cylinder and the Prandtl number are kept fixed as ϕ = 0oand Pr = 100. Numerical experiments in generalized body-fitted coordinates subject to Boussinesq approximation were conducted in the form of solution of continuity, momentum and energy equations. The momentum and energy equations are discretized using finite difference method. The equations are solved by using SMAC type implicit pressure correction scheme. The flow is noticed steady for 1 ≤ Re ≤ 30 and 0 ≤ Ri ≤ 0.50 at α = 0o, 1 ≤ Re ≤ 20 and 0 ≤ Ri ≤ 0.50at α = 45o, 1 ≤ Re ≤ 10 and 1.0 ≤ Ri ≤ 1.50 at α = 90o. Onset of vortex-shedding is observed initially at Re = 30, α = 45o, 0 ≤ Ri ≤ 0.50, the flow becomes unsteady and periodic flow. At small magnitudes of Reynolds number, the wake on downstream side of cylinder is found thin, and it becomes wider at large magnitudes of Reynolds number. It is noticed that the width of the wake reduces in size with increasing Richardson number. Maximum mean lift coefficient is found to occur at Re = 20, Ri = 1.5 and α = 90o, and maximum mean drag coefficient is noted at Re = 1 for the chosen range of Richardson number and free-stream orientations. For the whole range of Reynolds and Richardson numbers, the front face(s) of the cylinder had more crowding of isotherms in comparison with other faces of the cylinder. The front face(s) of the cylinder have high rate of heat transfer as compared to other cylinder faces. Heat transfer rate from the cylinder is enhanced either with increase in Richardson number or Reynolds number.

Keywords: Mixed convection, streamline and isotherms patterns, contours of vorticity, Nusselt number, rate of heat transfer.;

1. Introduction

The geometry of the cylindrical cross-section chosen in the present study is shown in Fig. 1, which affects the flow dynamics, wake properties and heat transfer characteristics significantly. In the past few decades, the fluid flow past bluff bodies of various cross-sections have been extensively examined, especially the cylindrical objects. Active and passive control methods are basically employed to control the vortex-shedding from bluff bodies. For a cylindrical object of square cross-section, the free-stream orientation is an important parameter, which affects the dynamics of flow considerably. In the present study, the mixed convective flow is considered as it is closer to real engineering applications such as tall buildings, chimneys, bridges, vortex generators etc. Electronic components, heat exchangers, extended surfaces, cooling towers are also important from the point of view of heat transfer. The present ploblem is closer to the engineering problems such as cooling of immersed assembly of core and windings in the oil in case of large electric transformers.Shell and tube oil cooler that is used for cooling of hydraulic power packs and hydraulic equipment like hydraulic systems on excavators and earthmoving equipment. Cooling of various electric and hybrid power train components in electric vehicles etc. In the present study, the effects of Re = 1, 5, 10, 20, 30, 40, 45 and Ri = 0, 0.25, 0.50, 1.0, 1.25, 1.50 on fluid dynamics and characteristics of heat transfer are analyzed at a fixed Prandtl number Pr = 100 and cylinder orientation ϕ = 0^o withthe range of orientations of the free-stream $0^o \leq \alpha \leq 90^o$. TheCPU time required for computations in this studyis 9072 hours.

The two-dimensional flow dynamics across an elevated square cylinder is considered in mixed convection by accounting Oberbeck-Boussinesq model. Variation of fluid properties in Oberbeck-Boussinesq model such as viscosity, specific heat, thermal diffusivity with temperature are ignored completely. The five dimensionless parameters that described the flow dynamics are as follows: the bluff-body orientation with respect to the x-axis = ϕ, Free-stream orientation with respect to gravity = α, Prandtl number (Pr) = $\frac{\nu_o}{\kappa_o}$, Richardson number (Ri) = $\frac{g\beta(T_s - T_\infty)d}{U_\infty^2}$ and Reynolds number (Re) = $\frac{U_\infty d}{\nu_o}$. Where ν_o = kinematic viscosity, κ_o = thermal diffusivity at a certain reference temperature (T_∞), T_s = uniform surface temperature of the bluff-body, T_∞ = fluid temperature of the free-stream, d =

* Corresponding author e-mail: rashidali1@zhcet.ac.in.

characteristic length scale of the body, β = co-efficient of volume expansion and g = gravitational intensity of the fluid.

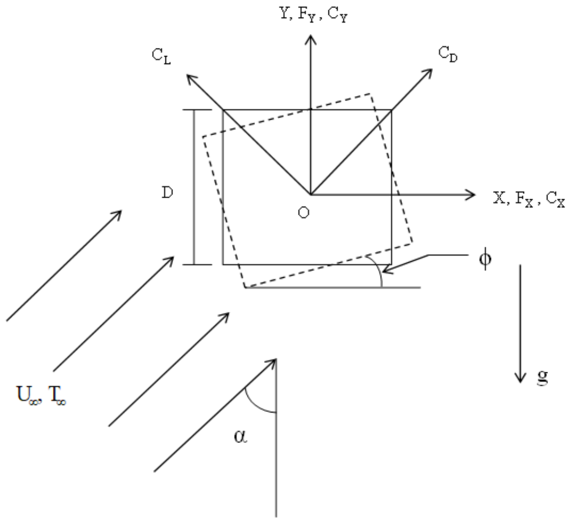

Figure 1. Geometry of the proposed problem with and without cylinder orientation (ϕ).

Sohankar et al. [1] investigated numerically a2-D, incompressible, unsteady air flow across a square cylinder for the conditions **$45 \leq Re \leq 200$,** $0 \leq \phi \leq 45^o$, $\alpha = 90^o$, **2.5%**$\leq$ BR $\leq$ 5% (BR = blockage ratio). They compared the boundary conditions and showed that the Neumann boundary condition was less effective than the convective Somerfield boundary condition in reducing the CPU time and upstream influence from the outlet of the computational domain. Sharma and Eswaran [2] studied numerically for parameters Re = 100, $-1 \leq Ri \leq 1$, $\alpha = 0^o$, $\phi = 0^o$, and Pr = 0.7, the heat transfer characteristics of two-dimensional flow across a cylinder of square cross section, the temperature of the cylinder is maintained constant. In energy equation, the viscous dissipation term is ignored completely and considered the effects of opposing and aiding buoyancy. They found that the shedding of vortices are completely suppressed at a critical Richardson number, Ri = 0.15. Sharma and Eswaran [3]numerically investigated the two-dimensional upward flow ($\alpha = 0^o$) by taking into account the opposing and aiding buoyancy, heat transfer characteristics across a cooled or heated square cylinder and the channel-confinement effect of different BR (BR = 10%, 30%, and 50%) for $-1 \leq Ri \leq 1$, Pr = 0.7, Re = 100, $\alpha = 0^o$ and $\phi = 0^o$. They noticed that the least heating required for vortex-shedding suppression decreases with increasing blockage ratio up to a certain value of BR (BR = 30%), and increases thereafter. Chatterjee and Mondal [4] investigated numerically the buoyancy (aiding/opposing) effects on the 2-D upward flow and heat transfer across a cooled or heated cylinder of square cross-section within the Boussinesq approximation at BR = 2%, $50 \leq Re \leq 150$, $-1 \leq Ri \leq 1$, Pr = 0.7and $\alpha = 0^o$. They observed that with increased heating there is an increment in Strouhal number and instantly falls to zero at some Richardson number (critical). They also noticed that with the increase in blockage ratio, the critical Richardson number was decreased.

Dhiman et al. [5] considered the upward, steady, confined flow in the vertical channel and investigate the characteristics of heat transfer for the flow around a square cylinder within the Boussinesq approximation, under aiding buoyancy at $1 \leq Re \leq 40$, $0 \leq Ri \leq 1$, Pr = 0.7 and 25% $\leq$ BR $\leq$ 50%. They reported that the onset of flow separation occurs at $2 \leq Re \leq 3$, 25% $\leq$ BR $\leq$ 30% and at $3 \leq Re \leq 4$, BR = 50%, irrespective of the value of Richardson number. Also, with increase in Re and Ri, the surface mean Nusselt number was increased. Yang and Wu [6], numerically studied the effects of opposing/aiding buoyancy and side ratio on 2-D flow and characteristics of heat transfer past a rectangular cylinder (cooled/heated) by adopting the Boussinesq approximation at $0.5 \leq SR \leq 2$ (SR = side ratio), $\alpha = 0^o$, $-1 \leq Ri \leq 1$, Pr = 0.7 and Re = 100. They noticed the Karman vortex-street for the flow conditions. They also noticed the complete suppression of vortex-shedding atRi = 0.15 and SR = 1. Moulai et al. [7] numerically investigated the mixed convective flow past a heated square cylinder under aiding buoyancy effect and heat transfer in air (Pr = 0.71), in a confined channel for the parameters $20 \leq Re \leq 45$ and $1.61x10^3 \leq Gr \leq 6.33x10^3$ at a fixed blockage ratio of 0.1. In their study, the strong dependency of wake region is observed on Grashof and Reynolds numbers. On decreasing the Grashof number and increasing the Reynolds number the wake region of square cylinder increase in their size. Enhancement of heat transfer from the front face of square cylinder is seen with increase in Reynolds number, and enhancement of heat transfer from the side faces of square cylinder is seen with increasing the Grashof number.

Rashid and Hasan [8] investigated numerically the phenomenon of vortex shedding and its suppression at Re = 100, Pr = 0.71, Ri and αranges chosen in the study are 0 to 1.6 and $0^o \leq \alpha \leq 90^o$. Rashid and Hasan [9] studied the influence of free-stream orientation and buoyancy on the flow structure and aerodynamic characteristics around a square cylinder for Re = 100, Pr = 0.71, $0^o \leq \alpha \leq 90^o$ and $1.2 \leq Ri \leq 1.6$. Rashid and Hasan [10] investigated numerically the effect of free-stream orientations and buoyancy together on flow structure and heat transfer in two-dimensional mixed convective flow past a square cylinder. The numerical experiments have been conducted at a fixed Reynolds number (Re) of 100 and Prandtl number (Pr) of 0.71. The Richardson number (Ri) ranges from 1.2 to 1.6, while free-stream orientation chosen in the range from 0^o to 90^o. Haider and Rashid [11] investigated numerically the effect of Prandtl number on the flow past a square cylinder in mixed convective flow regime at $0^o \leq \alpha \leq 90^o$, $0 \leq Ri \leq 1.6$, Pr = 0.7 and 7, Re = 100 and $\phi = 0^o$. Anshumaan and Rashid [12] studied numerically the effect of buoyancy and inertia forces on the flow and heat transfer characteristics for the conditions $1 \leq Re \leq 10$, $0 \leq Ri \leq 0.75$, Pr = 100, $\alpha = 90°$ and $\phi = 0°$. Rashid and Hasan [13] numerical investigated the transformations / bifurcations from steady to unsteady or unsteady to steady flow states in 2-D mixed convection across a square cylinder (heated) in laminar flow regime. The parameters chosen in their study were $0^o \leq \alpha \leq 90^o$ and $0 \leq Ri \leq 1.6$ and Pr = 0.71. The magnitudes of Reynolds and Richardson numbers were varied to obtain the neutral curves in Ri-α plane.

Yuan et al. [14] investigate numerically the flow patterns and vortex-shedding around a square cylinder using a control circular bar on upstream and downstream. The Lattice Boltzmann method (LBM) was used to investigate the flow over a square cylinder. Re = 100 for square cylinder, 30 and 50 for different circular bars were chosen (based on the width of the square cylinder (D) and diameter of circular bar (d)). The L/D and G/D ratios chosen were 1-5 (where L and G are the center-to-center distances between the bar and cylinder). They found that the maximum percentage reduction in drag coefficient was 59.86% by upstream control bar, and the maximum percentage reduction in rms lift coefficient was 73.69% by downstream control bar. Yuan et al. [15] numerically investigate the patterns of flow across a square cylinder with a circular bar upstream and a splitter plate downstream by Lattice Boltzmann method (LBM). The parameters chosen in their study were Re = 100 (based on side length of square cylinder (D)), Ds/D = 1-5, G/D = 0-7 and L/D = 1-6 (where *Ds*, *G* and *L* are the center-to center distance, surface-to-surface distance and the splitter plate length). They found that the maximum percentage reduction in mean drag coefficient was 68.76% at (*ds, g, l*) = (2.5, 0, 3)which was in pattern VI. The vortex-shedding from the square cylinder and the circular bar was completely suppressed in pattern VI. They also observed that the small distance between the square cylinder and the splitter plate plays a more vital role in suppression of vortex-shedding as compared with large distance and length. Rafik et al. [16] used the finite-volume method to investigate the laminar 2-D unsteady flow of nanofluids and heat transfer characteristics past a square cylinder inclined with respect to the main flow. The Reynolds number, nanoparticle volume fraction and inclination angle are chosen 100, 0-5% and 0^o-45^o, respectively. Enhancement of heat transfer is reported in their study with nanoparticles addition. It is also reported that by increasing the nanoparticles concentration for a specific inclination angle the local Nusselt number increases.

The survey of the earlier studies suggested that none of the previous studies have been carried out to investigate the effects of buoyancy and free-stream orientations on fluid dynamics and heat transfer characteristics for the flow past a heated square cylinder for the ranges of parameters, Reynolds number, $1 \leq Re \leq 45$, Richardson number, $0 \leq Ri \leq 1.50$, Prandtl number, Pr = 100, cylinder orientation, $\phi = 0^o$ and orientation of free-stream, $\alpha = 0^o$, 45^o and 90^o. The focus of the present study is to elucidate the role of Reynolds and Richardson numbers, and free-stream orientations on time histories of lift and drag coefficients, streamline patterns, contours of vorticity, isotherm patterns, mean (time mean) lift and drag coefficients (C_L and C_D), time mean coefficient of moment (C_M), surface pressure and surface vorticity. In addition, the local Nusselt number (Nu_L) and mean (time mean) Nusselt number (Nu) are investigated in detail. The novelty of the present work is the solution of complex problem of bluff-body numerically with the consideration of range of Richardson number, Reynolds number and orientation of free-stream. In the knowledge of the author no study of flow past bluff-body is found till date with these range of parameters, specifically the free-stream orientations range.

2. . MATHEMATICAL FORMULATION

In the current study, the fluid flow is considered as unsteady, 2D, incompressible, laminar and viscous across an elevated square cylinder. The buoyancy impacts are considered by the Oberbeck-Boussinesq model approximation (Tritton[17]). The equations involving continuity, momentum and energy have been written in the following form;

Continuity Equation

$$\nabla.\vec{V} = 0 \tag{1}$$

Momentum Equation

$$\frac{D\vec{V}}{Dt} = -\frac{1}{\rho_\infty}\nabla P + \nu_\infty \nabla^2 \vec{V} - \vec{g}\beta\left(T - T_\infty\right) \tag{2}$$

Energy Equation

$$\frac{\partial T}{\partial t} + \vec{V}.\nabla T = \kappa_\infty \nabla^2 T \tag{3}$$

In the above equations (1)-(3), T, P and $\vec{V}$ are the temperature, pressure and the vector of local fluid speed. The density, thermal diffusivity as well as the kinematic viscosity at free-stream reference temperature (T_∞) are ρ_∞, κ_∞ and ν_∞, respectively. Figure 1 shows the proposed problem geometry considered in the present study. In figure 1, forces/span are $F_x$in x direction and $F_y$in x and y direction, C_L and C_D are the lifting and dragging coefficients, respectively with reference to orientation of free-stream. U_∞ is the free-stream velocity, ϕ is the cylinder orientation, d is the edge of square cylinder and g is the gravitational intensity.

The initial condition in the flow region are selected to be the free-stream variables written as,

$$P = P_\infty, \quad T = T_\infty, \quad \vec{V} = U_\infty = \left(Sin\alpha\,\hat{i} + Cos\alpha\,\hat{j}\right). \tag{4}$$

The unit vectors in the x and y directions are $\hat{i}$ and $\hat{j}$ in the above relation.

Condition of no-penetration &no-slip are used as boundary conditions for the component of velocity on the square cylinder surface, the square cylinder surface is maintained at higher constant temperature T_s

$$\vec{V} = 0, \quad T = T_s. \tag{5}$$

Normal momentum condition at the cylinder surface is used for pressure. At large distances from the cylinder, the uninterrupted free-stream conditions are used.

Mathematical equations of mass, momentum and energy are transformed into dimensionless form, with the time scales; velocity and length chosen are,

i) Time scale $\equiv$ 'd/U_∞' = residence time spend by fluid particles in the neighborhood of the cylinder.

Non-dimensional time and velocities are written as,

$$\tau = tU_\infty/d, \; u = U/U_\infty \text{ and } v = V/U_\infty. \tag{6}$$

ii) Velocity scale $\equiv$ 'U_∞' = magnitude of the velocity of free-stream.

iii) Length scale $\equiv$ 'd' = side of square cylinder.

Fluid temperature change scale is($T_s - T_\infty$)&change in pressure scale is $\rho_o U_\infty^2$, and the non-dimensional pressure and temperature are written as,

$$\bar{p} = \frac{P - P_\infty}{\rho U_\infty^2}, \theta = \frac{T - T_\infty}{T_s - T_\infty}. \tag{7}$$

Mass, momentum and energy equations in dimensionless form with Oberbeck-Boussinesq approximation in Cartesian coordinates, modified into generalized body-fitted coordinates (Thompson et al. [18]) are written as,

Continuity:

$$\left(\xi_x \frac{\partial}{\partial\xi} + \eta_x \frac{\partial}{\partial\eta}\right)u + \left(\xi_y \frac{\partial}{\partial\xi} + \eta_y \frac{\partial}{\partial\eta}\right)v = 0, \tag{8}$$

x – Momentum:

$$\frac{\partial u}{\partial \tau}+U^{\xi}\frac{\partial u}{\partial \xi}+U^{\eta}\frac{\partial u}{\partial \eta}=-\left(\xi_x\frac{\partial \bar{p}}{\partial \xi}+\eta_x\frac{\partial \bar{p}}{\partial \eta}\right)+\frac{1}{Re}\tilde{\nabla}^2 u, \quad (9)$$

y – Momentum:

$$\frac{\partial v}{\partial \tau}+U^{\xi}\frac{\partial v}{\partial \xi}+U^{\eta}\frac{\partial v}{\partial \eta}=+Ri\theta-\left(\xi_y\frac{\partial \bar{p}}{\partial \xi}+\eta_y\frac{\partial \bar{p}}{\partial \eta}\right)+\frac{1}{Re}\tilde{\nabla}^2 v \quad (10)$$

Energy Equation:

$$\frac{\partial \theta}{\partial \tau}+U^{\xi}\frac{\partial \theta}{\partial \xi}+U^{\eta}\frac{\partial \theta}{\partial \eta}=\frac{1}{(Re.Pr)}\tilde{\nabla}^2\theta. \quad (11)$$

The corresponding non-dimensional Cartesian velocity components in the above equations are u and v. Dimensionless components of velocity are referred to as U^{ξ} and U^{η} in ξ and η directions. The body-fitted velocity coordinate components are connected to the Cartesian components as,

$$U^{\xi}=\xi_x u+\xi_y v, \quad (12)$$

$$U^{\eta}=\eta_x u+\eta_y v. \quad (13)$$

$\tilde{\nabla}^2$ is the transformed Laplacian operator written as,

$$\tilde{\nabla}^2 \equiv \tilde{A}\frac{\partial^2}{\partial \xi^2}+2\tilde{B}\frac{\partial^2}{\partial \xi \partial \eta}+\tilde{C}\frac{\partial^2}{\partial \eta^2}+\tilde{P}\frac{\partial}{\partial \xi}+\tilde{Q}\frac{\partial}{\partial \eta} \quad (14)$$

Coefficients $\tilde{A},\tilde{B},\tilde{C},\tilde{P}$, and $\tilde{Q}$ are,

$$\tilde{A}=\xi_x^2+\xi_y^2,\ \tilde{B}=\xi_x\eta_x+\xi_y\eta_y,\ \tilde{C}=\eta_x^2+\eta_y^2 \quad (15)$$

and,

$$\nabla^2\xi=\tilde{P},\ \ \nabla^2\eta=\tilde{Q}. \quad (16)$$

the Laplacian ∇^2 in the Cartesian coordinates are written as,

$$\nabla^2 \equiv \frac{\partial^2}{\partial x^2}+\frac{\partial^2}{\partial y^2}. \quad (17)$$

2.1. Boundary conditions

Condition of no-penetration and no-slip is used for components of velocity at the rigid surface of a square cylinder. $\theta=1.0$ is used for temperature on the cylinder surface. The normal momentum equation is employed for pressure on the rigid cylinder surface,

$$\frac{\partial \bar{p}}{\partial \eta}=\frac{\partial \bar{p}}{\partial x}\frac{\partial x}{\partial \eta}+\frac{\partial \bar{p}}{\partial y}\frac{\partial y}{\partial \eta} \quad (18)$$

where, $\frac{\partial \bar{p}}{\partial x}$ and $\frac{\partial \bar{p}}{\partial y}$ on the surface of cylinder are found from the momentum equations of x and y.

The artificial boundary is split into two portions to enforce the boundary conditions. One portion is the inflow and the other portion is the outflow. This is accomplished by controlling the local normal velocity variable direction. For a typical outer surface normal pointing towards the inside of the flow domain $\vec{U}.\hat{n}>0$ implies inflow and $\vec{U}.\hat{n}<0$ implies outflow. The boundary conditions on both the portions are written as

The inflow Portion

Uninterrupted free-stream conditions for speed and temperature are enforced at the inflow part, written as,

$$\theta=0,\quad \bar{p}=0,\quad \vec{U}=Sin\alpha\,\hat{i}+Cos\alpha\,\hat{j}. \quad (19)$$

Pressure is update by implementing the normal momentum equation.

The outflow Portion

Hasan et al. [19] proposes a numerical boundary condition for velocities at the outflow portion, this is executed in the present study. They utilizes vorticity considerations and mass conservation for incompressible flows to extrapolate the radial decay laws for the deviation / perturbation in circumferential and radial velocities created due to the presence of a body in an otherwise uniform undisturbed stream. They reported that by using their outflow velocity condition for domains comparatively smaller sizes, the precise computations would be carried out easily. The presence of the body causes deviations to the circumferential and radial velocity components are shown to obey radial decay laws with a leading order term written as (Hasan et al. [19]),

$$v_r-v_{r\infty}\sim S_1/r^2$$

$$v_\theta-v_{\theta\infty}\sim \left.\begin{array}{ll} S_2/r^2 & \text{if } \Gamma=0 \\ S_2/r & \text{if } \Gamma\neq 0\end{array}\right\}. \quad (20a)$$

The local circumferential and radial free-stream components are represented as $v_{\theta\infty}$ and $v_{r\infty}$, respectively, these components are obtained from the Cartesian free-stream velocity components. The circulation on the artificial boundary in the above equation is represented by the symbol 'Γ', which can be estimated from the existing velocity field. The constants S_1 and S_2 are obtained by interpolating the values of the deviations in the circumferential and radial velocity components at an interior point (i). Thus, the circumferential and the radial velocity components on the artificial boundary at a point (B) would be determined using equations (20a) as,

$$(v_r)_B \sim (v_r-v_{r\infty})_i\left\{r_i^2/r_B^2\right\}+(v_{r\infty})_B,$$

$$(v_\theta)_B \sim \left.\begin{array}{ll} (v_\theta-v_{\theta\infty})_i\left\{r_i^2/r_B^2\right\}+(v_{\theta\infty})_B & \text{if } \Gamma=0 \\ (v_\theta-v_{\theta\infty})_i\left\{r_i/r_B\right\}+(v_{\theta\infty})_B & \text{if } \Gamma\neq 0\end{array}\right\} \quad (20b)$$

These components can then be utilized for obtaining the Cartesian components u, v.A derivative of second order for temperature in η direction is used, written as,

$$\frac{\partial^2\theta}{\partial \eta^2}=K_2 \quad (20c)$$

At an interior point, K_2 is the magnitude of 2nd order derivative and uses the 2nd order backward difference scheme.

The boundary condition (traction free) of [20] and [21] is used for pressure, written as,

$$\bar{p}=\frac{1}{Re}\frac{\partial U^n}{\partial n}. \quad (21)$$

In the above equation the local normal is represented by n and the local normal velocity is U^n.

2.2. Grid structure

In the current research, a mesh that is uniform in ξ and η directions is taken into account in the mapped computational ξ-η plane. The spacing of mesh $(\Delta\xi \text{ and } \Delta\eta)$ is assigned in terms of fixing the number of mesh points in the required (ξ and η) directions. The body-fitted coordinates $\xi(x, y)$ and $\eta(x, y)$ are chosen for the mapping of grid points in the physical plane to satisfy the Laplacian equations in the physical domain ($\tilde{P} = \tilde{Q} = 0$) written as,

$$\nabla^2\xi = 0, \ \nabla^2\eta = 0. \tag{22}$$

Mapped/inverted equations in the computational ξ-η domain are given as,

$$D\frac{\partial^2 x}{\partial\xi^2} - 2E\frac{\partial^2 x}{\partial\xi\partial\eta} + F\frac{\partial^2 x}{\partial\eta^2} = 0, \tag{23}$$

$$D\frac{\partial^2 y}{\partial\xi^2} - 2E\frac{\partial^2 y}{\partial\xi\partial\eta} + F\frac{\partial^2 y}{\partial\eta^2} = 0. \tag{24}$$

In Eqs. (23)-(24) D, E, F are,

$$D = \left(\frac{\partial x}{\partial\eta}\right)^2 + \left(\frac{\partial y}{\partial\eta}\right)^2,$$

$$E = \left(\frac{\partial x}{\partial\xi}\right)\left(\frac{\partial x}{\partial\eta}\right) + \left(\frac{\partial y}{\partial\xi}\right)\left(\frac{\partial y}{\partial\eta}\right) \text{ and} \tag{25}$$

$$F = \left(\frac{\partial x}{\partial\xi}\right)^2 + \left(\frac{\partial y}{\partial\xi}\right)^2.$$

Discretization of Eqs. (23) - (24) on uniform grid $(\Delta\xi, \Delta\eta)$ is done in computational plane in order to achieve grid in physical plane. An identical number of grid points are placed initially on the cylinder surface and finally on the artificial boundary, which corresponds to the number of mesh points in the computational plane in ξ direction. For elliptic Eqs. (23) - (24), the said boundary points function as Dirichlet boundary condition. The discrete solution of Eqs. (23)-(24) need a quasi-linear approach, as the equations are not linear to the undefined grid point coordinates (x, y). In the quasi-linearized method the D, E and F coefficients are discretized using the previous iterates, and the derivatives $\frac{\partial^2 x}{\partial\xi^2}, \frac{\partial^2 x}{\partial\xi\partial\eta}, \frac{\partial^2 x}{\partial\eta^2}, \frac{\partial^2 y}{\partial\xi^2}, \frac{\partial^2 y}{\partial\xi\partial\eta}$ and $\frac{\partial^2 y}{\partial\eta^2}$ are discretized using current/new iterates with finite difference schemes of second order (central). The corresponding linear algebraic set of equations were solved using Gauss-Seidel method to extract the new iterates from existing previous values. One Gauss-Seidel sweep is used per iteration for the two discretized equations (23)-(24). In previous study of Rashid and Hasan [13], the comprehensive analysis of grid structure is discussed.

The methodology constituting the generation of an O-type structured grid, numerical scheme utilized in present study, boundary conditions at cylinder's solid surface and on the artificial boundary (outflow/inflow portions) are elaborated in detail in the previous studies of Rashid and Hasan [13] Hasan and Rashid [22]. For pressure correction, scheme identical to SMAC scheme is utilized which is elaborated in the study of Hasan and Sanghi [23]& Hasan et al. [19]. The discretization of governing equations of mass and momentum is done by employing spatial discretization of finite difference type on a non-staggered body-fitted grid. In the interior, a fourth-order central scheme is employed for diffusion terms, while for the convection terms a hybrid scheme of third-order upwind scheme (Kunio Kuwahara [24]) and fourth-order central is employed. For near boundary points (artificial and solid), second-order central schemes are employed for both convection and diffusion terms. For pressure interpolation, the concept of Rhie and Chow [25] is utilized.

2.3. Dimensionless output parameters

From application perspective, the influence of flow across a body is described in terms of the gross quantities, such as the moments or forces the fluid exerts on the object, and the overall rate of heat transfer between the fluid and the body. All such global parameters are described below in a dimensionless manner for the two-dimensional problem that is considered in the present study,

1. $C_L = C_y \sin\alpha - C_x \cos\alpha$, (Lift coefficient),
2. $C_D = C_x \sin\alpha + C_y \cos\alpha$, (Drag coefficient),
3. $C_M = 2M/\rho_o U_\infty^2 d^2$, (Moment coefficient),
4. $Nu = Q/[4k_o(T_s - T_\infty)]$, (Nusselt number),
5. $St = fd/U_\infty$. (Strouhal number).

C_y, C_x in the above equations are coefficients of forces in y and x directions given as,

$$C_x = \frac{2F_x}{\rho_o U_\infty^2 d} \text{ and } C_y = \frac{2F_y}{\rho_o U_\infty^2 d}. \tag{26}$$

F_x and F_y are the forces per unit cylinder span in x and y directions, respectively (Fig. 1). M is the overall moment the fluid exerted on the cylinder per unit span. Q is the maximum rate of heat transfer per unit cylinder span, and k_o is the fluid's thermal conductivity. The vortex-shedding frequency is expressed by 'f'.

The force coefficients in dimensionless form are,

$$C_x = 2\int_0^1 \bar{J}\bar{p}\bar{\eta}_x d\xi + \frac{2}{Re}\int_0^1 \bar{J}\bar{\Omega}\bar{\eta}_y d\xi, \tag{27}$$

$$C_y = 2\int_0^1 \bar{J}\bar{p}\bar{\eta}_y d\xi - \frac{2}{Re}\int_0^1 \bar{J}\bar{\Omega}\bar{\eta}_x d\xi, \tag{28}$$

$$C_M = 2\int_0^1 \bar{J}\bar{p}\left(\bar{x}\bar{\eta}_y - \bar{y}\bar{\eta}_x\right)d\xi - \frac{2}{Re}\int_0^1 \bar{J}\bar{\Omega}\left(\bar{x}\bar{\eta}_x + \bar{y}\bar{\eta}_y\right)d\xi. \tag{29}$$

The Fourier's law of heat conduction is utilized to find out the heat transfer rate from the cylinder written as,

$$q = -\oint k \frac{\partial T}{\partial n} b dl. \tag{30}$$

Heat transfer rate / unit width 'b' is calculated as,

$$\frac{q}{b} = -\oint k \frac{\partial T}{\partial n} dl. \tag{31}$$

Nusselt number is represented as,

$$Nu = \frac{q/b}{4k_o \left(T_s - T_\infty\right)}. \tag{32}$$

Nusselt number in dimensionless form is written as,

$$Nu = \frac{1}{4}\int_0^1 \bar{J} \frac{\partial \theta}{\partial \eta}\left(\bar{\eta}_x^2 + \bar{\eta}_y^2\right) d\xi. \tag{33}$$

2.4. Location of artificial boundary, grid size and time step selection

For finding out a suitable artificial boundary position, such that the numerical boundary conditions imposed on it does not affect considerably the dynamics of flow adjacent to the square cylinder. This is done by truncating the original grid with artificial boundary from the middle of the cylinder at a dimensionless distance of 120. The original grid of 241 x 325 mesh points is then truncate from the middle of the cylinder at dimensionless lengths of 100, 80, 60, 40 and 20 to give six numerical grids of equal grid cell size. For every truncated grid and at $\phi = 0^o$, Pr = 0.71, Re = 100, Ri = 0 and $\alpha = 0^o$, the Strouhal number, mean drag and lift coefficients are obtained from the numerical experiments. It is observed that change in the values of the lift coefficient are marginal for a dimensionless distance beyond 20 and change in the magnitudes of coefficient of drag and St beyond a dimensionless distance of 40 are quite small, and the length beyond 40 appears to be ideal for computations. The artificial boundary is positioned at a dimensionless distance of 40 from the middle of the cylinder for all subsequent reported computations. For the forced flow regime, the effects of grid size is analyzed by setting the far boundary at a distance of 40 from the middle of the square cylinder for Re = 45, Pr = 100, $\alpha = 90^o$, $\phi = 0^o$ and using a time step of 0.001 dimensionless units. Numerical experiments were conducted on3 grids of 161 x 179 (G1), 241 x 258 (G2) & 321 x 338 (G3) mesh points for the close boundary spacing of 0.0197, 0.0137 & 0.0104, respectively. The drag coefficient (mean), Strouhal number & Nusselt number (mean) for a free-stream orientation of 90^o are reported in Table 1 at various grid sizes. In moving from grid G1 to G2 the %age variation in the flow parameters including drag coefficient (mean), Strouhal number & Nusselt number (mean) is 0.275, 0.197 & 1.451, and in moving from grid G2 to G3 the %age variation is 0.701, 0.196 & 1.488, respectively. The outcome shows clearly that the %age variation in the flow parameter is very small (less than 1.5 percent) when moving from coarser to finer grid. Hence, the grid 241 x 258 (G2) is considered suitable for computations in order to conserve computational time.

Table 1. Grid size sensitivity for square cylinder at Re = 45, Pr = 100, Ri = 0 and $\alpha = 90^o$.

Grid	Near boundary spacing for the grid	Grid Size	$\bar{C}_D$	St	$\overline{Nu}$
G1	0.0197	161 x 179	1.5631	0.2030	17.6021
G2	0.0137	241 x 258	1.5588	0.2034	17.3503
G3	0.0104	321 x 338	1.5479	0.2038	17.0958

In order to determine the appropriate time step, the calculations were done in the forced & mixed convection regimes at the time steps of 0.0005 and 0.001 for Re = 45, Pr = 100, $\alpha = 90^o$ and $\phi = 0^o$. In Table 2 the drag coefficient (mean), Strouhal number & Nusselt number (mean), are compared for Richardson numbers 0 and 1.5 at different time steps. Moving from a time step of 0.0005 to 0.001 in the forced flow regime, the %age variation observed is 0.532, 0.098 & 0.811, respectively in the drag coefficient, Strouhal number& Nusselt number.

Table 2. Time step sensitivity for $\alpha = 90^o$, $\phi = 0^o$, Re = 45, Pr = 100 at Ri = 0 and 1.5.

Richardson number	Time step ($\Delta\tau$)	$\bar{C}_D$	St	$\overline{Nu}$
Ri = 0	0.0005	1.5671	0.2036	17.4911
	0.001	1.5588	0.2034	17.3503
Ri = 1.5	0.0005	1.6341	0.2587	17.6798
	0.001	1.6299	0.2583	17.7566

The %age variation in drag coefficient (mean), Strouhal number & Nusselt number (mean) in mixed convection at Ri = 1.5 is 0.257, 0.154 & 0.434, respectively. From the above discussion, it is suggested that minor span has no noticeable effect on the performance (<1 %). So a time step of 0.001 is selected for all the computations.

3. CODE VERIFICATION AND VALIDATION

Checking of numerical method, selection of numerical parameters, and the code used for numerical simulation is verified and validated by examining the present results with those reported in previous studies with in the forced and mixed convection. Numerical simulations were performed at $\alpha = 90^o$, $\phi = 0^o$, Re = 5, Pr = 100 and $0 \le Ri \le 0.50$. It is depicted in Table 3 that the present results of mean (time mean) drag coefficient (C_D) obtained from computations is in agreement with results reported in the earlier studies of Dhiman et al. [26], Paliwal et al. [27] and Dhiman et al. [28]. Computations have been carried out for the conditions, Re = 5, Pr = 100, Ri = 0.0 and $\alpha = 90^o$. It is seen from Table 4 that the present result of mean Nusselt number (Nu) is in agreement with the results of Dhiman et al. [28], Paliwal et al. [27] and [29] [30] [31].

Table 3. Mean drag coefficient (C_D) at Re = 5, Pr = 100, Ri = 0.0, 0.25, 0.50 and α = 90°

	Ri = 0.0	Ri = 0.25	Ri = 0.50	
Dhiman et al. [26]	4.840			Numerical
Paliwal et al. [27]	4.814			Numerical
Dhiman et al. [28]		4.686	4.729	Numerical
Present Study	4.364	4.377	4.405	

Table 4. Mean Nusselt number (Nu) at Re = 5, Pr = 100, Ri = 0.0 and α = 90°

	Nu	
Dhiman et al. [28]	5.504	Numerical
Paliwal et al. [27]	5.723	Numerical
Present Study	5.370	

Table 5. Comparison of $\overline{C}_{L,r.m.s}$, $\overline{C}_D$, $\overline{Nu}$ and St for square and circular cylinders at Ri = 0, Re = 100 and Pr = 0.71.

	Cylinder	$\overline{C}_{L,r.m.s}$	$\overline{C}_D$	$\overline{Nu}$	St
Experimental					
Okajima [32] α = 90°	Square	-	-	-	0.141-0.145
Luo et al. [33] α = 90°	Square	-	-	-	0.146
Collis and Williams [34] α = 90°	Circular	-	-	5.160	
Wang and Travnicek [35] α = 90°	Circular	-	-	5.101	
Wang et al. [36] α = 90°	Circular	-	-	-	0.161
Numerical					
Sohankar et al. [1] α = 90°	Square	0.139	1.460	-	0.146
Saha et al. [37] α = 90°	Square	-	1.510	-	0.159
Sharma and Eswaran [2] α = 0°	Square	0.183	1.559	4.070	0.148
Ranjan et al. [38] α = 90°	Square	0.190	1.449	4.124	0.145
Yoon et al. [39] α = 90°	Square	0.179	1.428	-	-
Present (α = 0°)	Square	0.175	1.438	4.051	0.143
Present (α = 90°)	Circular	-	1.316	5.240	0.163

The discrepancies between present results and the previous results of Dhiman et al. [26], Paliwal et al. [27] and Dhiman et al. [28] reported in Table 3 and 4 are found due to the slight differences in the numerical procedures adopted and the level of accuracy of the discrete solutions chosen. In the previous studies of [26], [27] and [28] uses a confined flow field structure (channel flow with slip conditions) while in the current study the flow field is chosen to be unconfined. The boundary conditions chosen by [26], [27] and [28] are different from the present study. In the studies of [26] and [28] finite volume method is utilized, and in the present study finite difference method is used. So it is difficult to get identical results with different numerical procedures, resulting in discrepancies in the results.

Table 5 compares the mean drag coefficient, rms lift coefficient, Strouhal number and mean Nusselt number, obtained in the current analysis with the data reported in earlier studies for circular and square cylinders at ϕ = 0°, Ri = 0, Pr = 0.71 and Re = 100. The data obtained from the current simulations are in close agreement with those obtained in the previous numerical and experimental studies. Present data of Strouhal number is in close relation with the data reported for both circular and square cylinders in earlier experimental studies.

4. RESULTS AND DISCUSSION

The current study is carried out for the range of parameters $1 \le Re \le 45$, $0 \le Ri \le 1.50$, $0^o \le \alpha \le 90^o$ at a fixed ϕ = 0° and Pr = 100. Effects of Reynolds and Richardson numbers and orientation of the free-stream on patterns of streamline, vorticity contours, patterns of isotherm, non-dimensional time histories of drag and lift coefficients, mean (time mean) drag and lift coefficients (C_L and C_D), mean coefficient of moment (C_M), surface pressure and surface vorticity, local Nusselt number (Nu_L) and mean Nusselt number (Nu) have been carried out in detail.

4.1. Streamline Patterns, Contours of Vorticity and Isotherm Patterns

Patterns of streamline, vorticity contours and patterns of isotherm are depicted in Figs. 2-10for $1 \le Re \le 45$, $0 \le Ri \le 1.50$, $0^o \le \alpha \le 90^o$, ϕ = 0° and Pr = 100. It is seen from patterns of streamlines(Fig. 2-Fig. 4) and contours of vorticity (Figs. 5-7) that no vortices are formed at Re = 1 for the range of free-stream orientations and Richardson number chosen. The vortices are induced at higher magnitudes of Reynolds number, and further increases in their size with increase in Reynolds number. Similar trends are observed for the range of free-stream orientations chosen. With the increase in Richardson number the vortices are reduced in their size and the wake becomes thin as depicted in Figs. 2-7. Due to the fact that there is variation in density in the buoyancy term with increasing Richardson number, the incoming free-stream fluid near cylinder got accelerated with increase in Ri, accelerates the shear layer leading to less entrainment of fluid to the vortices from shear layers and hence the vortices are reduced in their size. Increase in Ri enforces thermal energy diffusion in the near wake of the cylinder which creates stabilizing buoyant forces with respect to the ambient fluid just outside the shear layer. The buoyancy induced current tends to stabilize the flow, thus thinning of wakes takes place. Figures. 2-7 depicted that, at a fixed Ri with increasing Re, the wakes became wider behind the cylinder because of high rate of momentum transfer to the fluid particles at higher Re. Also the entrainment of the fluid to the vortices increases with increasing Reynolds number.

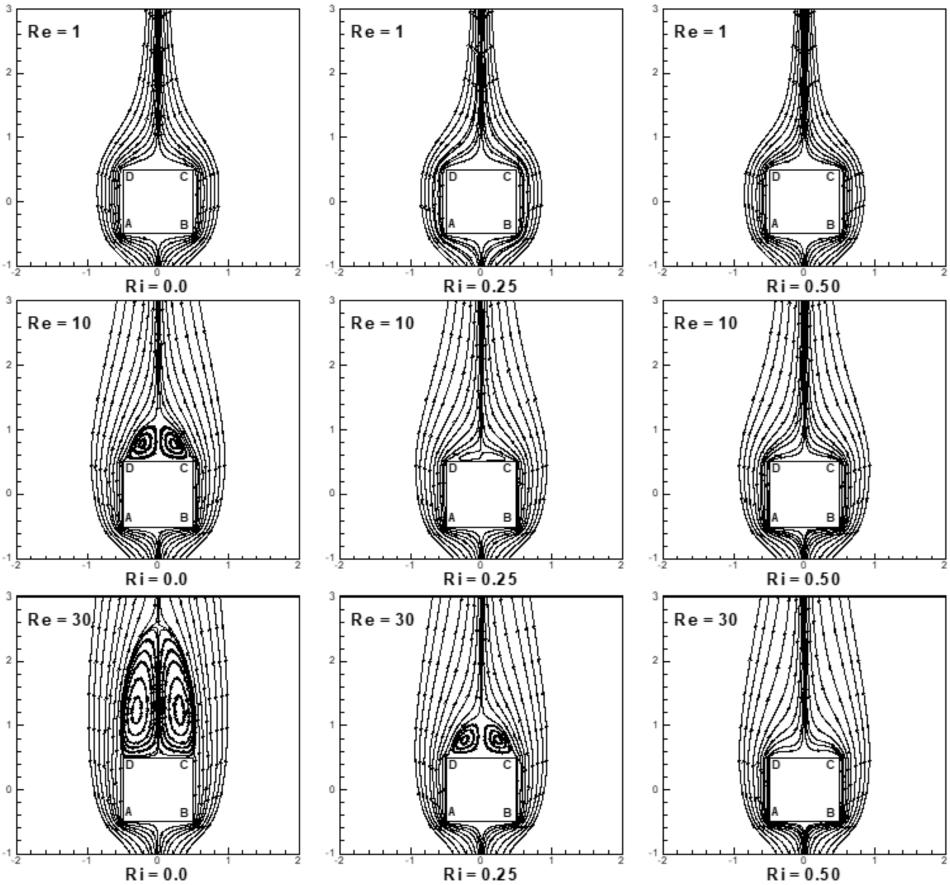

Figure 2. Streamline patterns for $1 \leq Re \leq 30$, $0 \leq Ri \leq 0.50$, $\alpha = 0^o$, at $Pr = 100$.

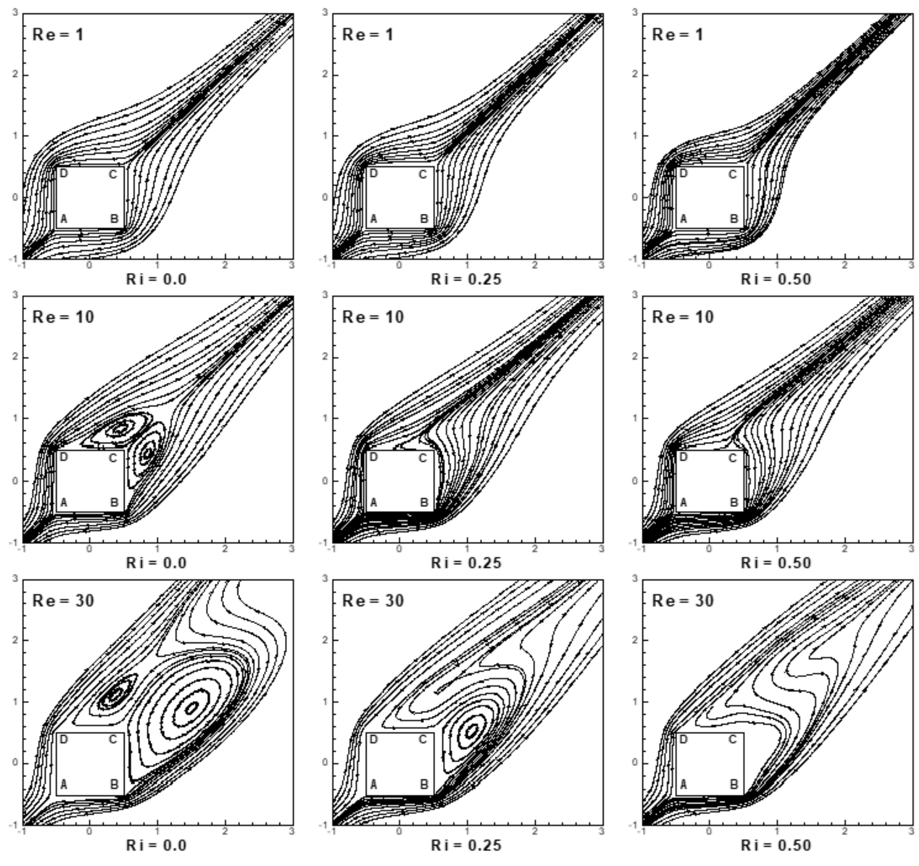

Figure 3. Streamline patterns for $1 \leq Re \leq 30$, $0 \leq Ri \leq 0.50$, $\alpha = 45^o$, at $Pr = 100$.

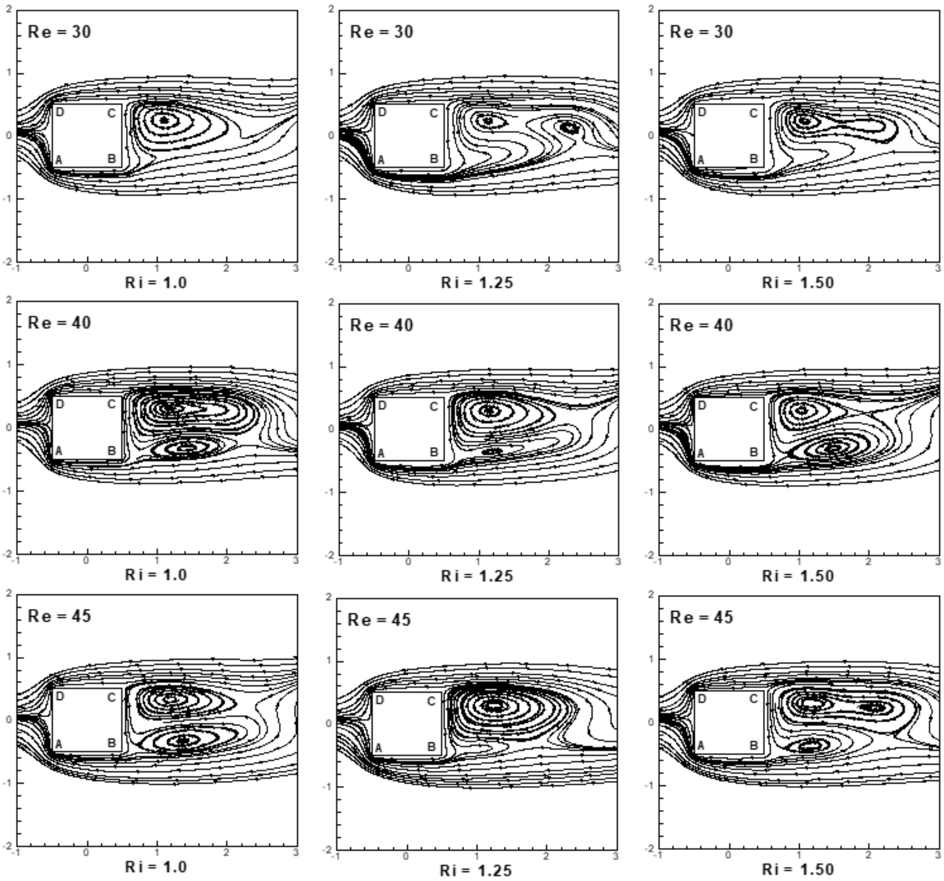

Figure 4. Streamline patterns for $30 \leq Re \leq 45$, $1.0 \leq Ri \leq 1.50$, $\alpha = 90^o$, at $Pr = 100$.

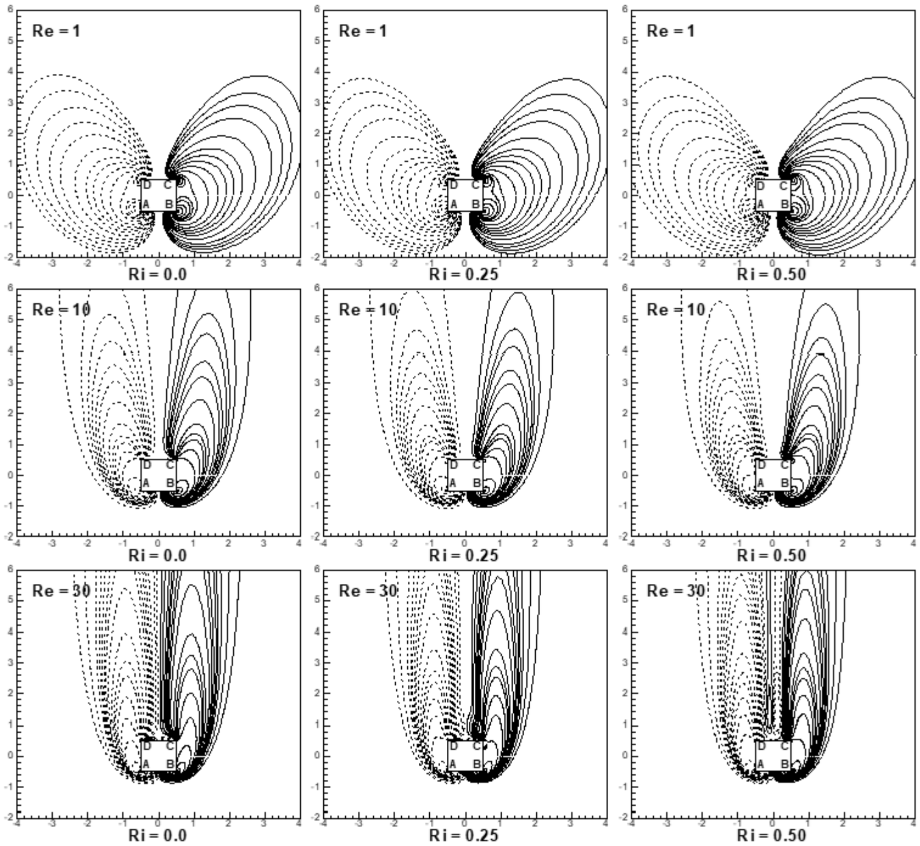

Figure 5. Contours of vorticity for the conditions ($Pr = 100$, $\alpha = 0^o$, $1 \leq Re \leq 30$, $0 \leq Ri \leq 0.50$).

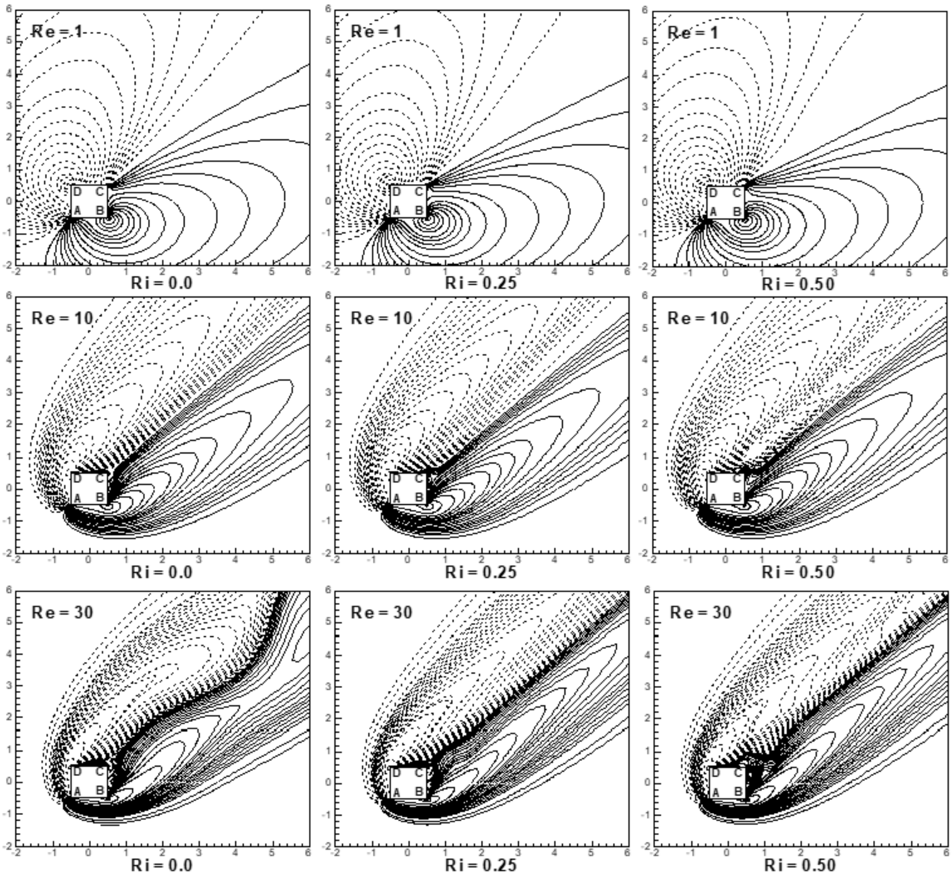

Figure 6. Contours of vorticity for the conditions (Pr = 100, α = 45°, 1 ≤ Re ≤ 30, 0 ≤ Ri ≤ 0.50).

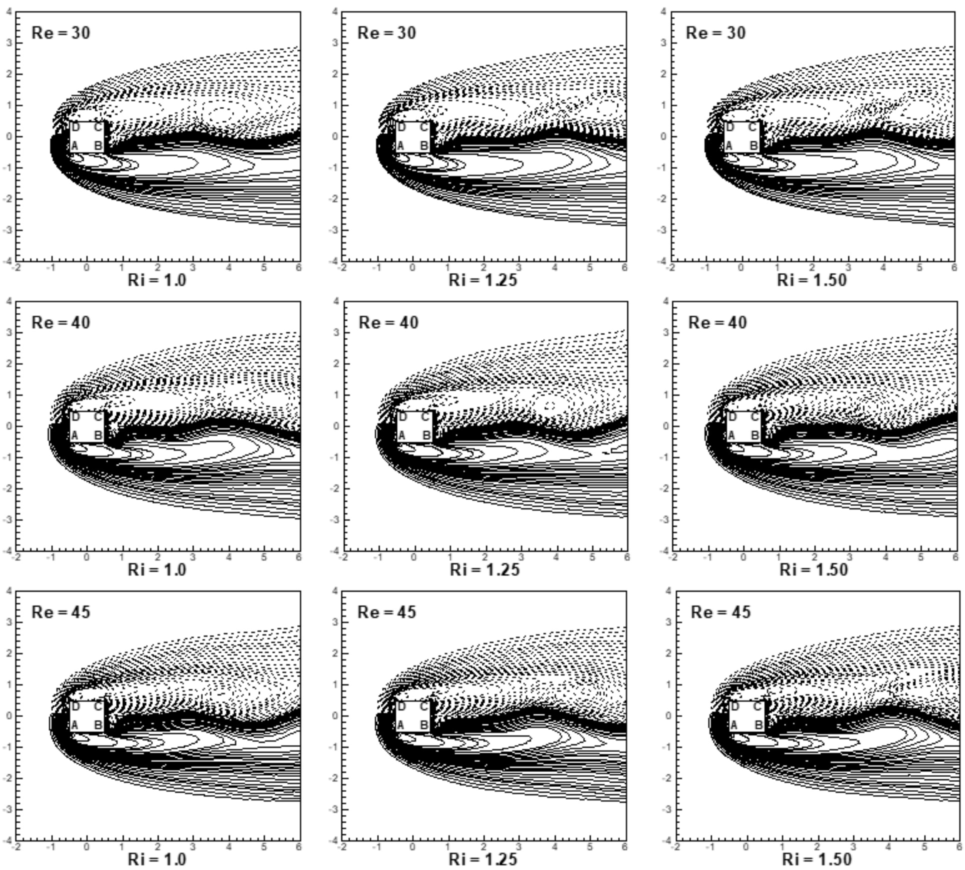

Figure 7. Contours of vorticity for the conditions (Pr = 100, α = 90°, 30 ≤ Re ≤ 45, 1.0 ≤ Ri ≤ 1.50).

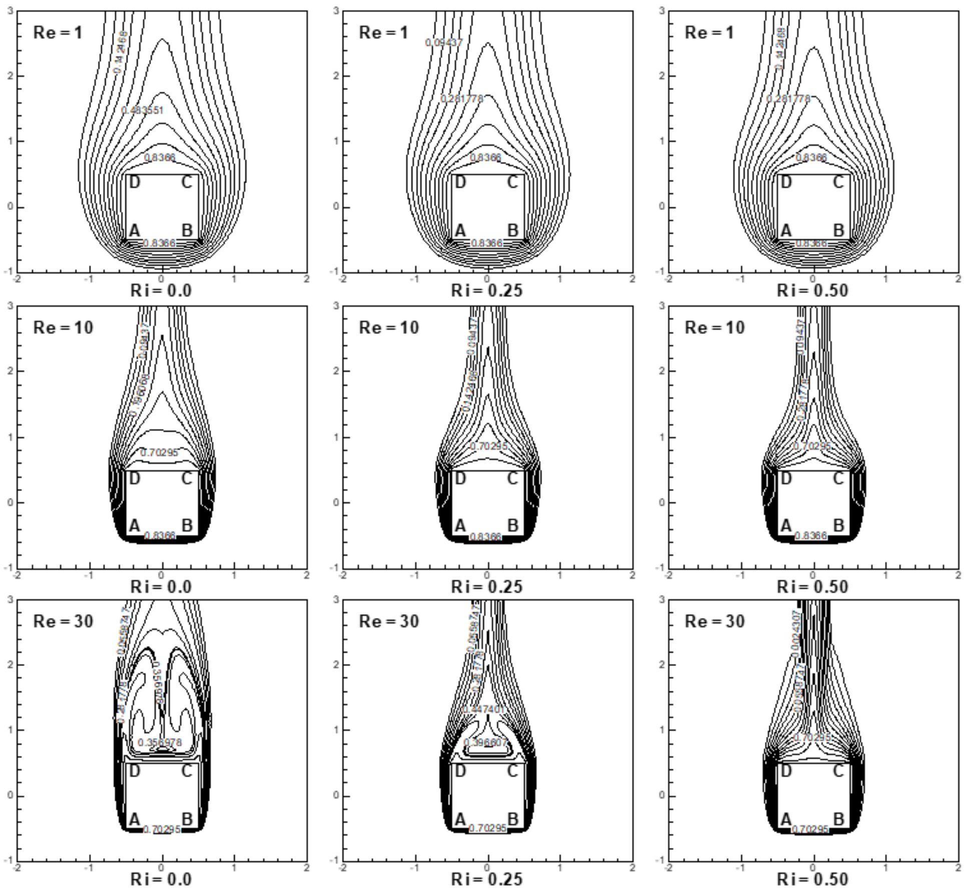

Figure 8. Isotherm patterns at Pr = 100, α = 0º, Re = 1, 10, 30 and Ri = 0.0, 0.25, 0.50.

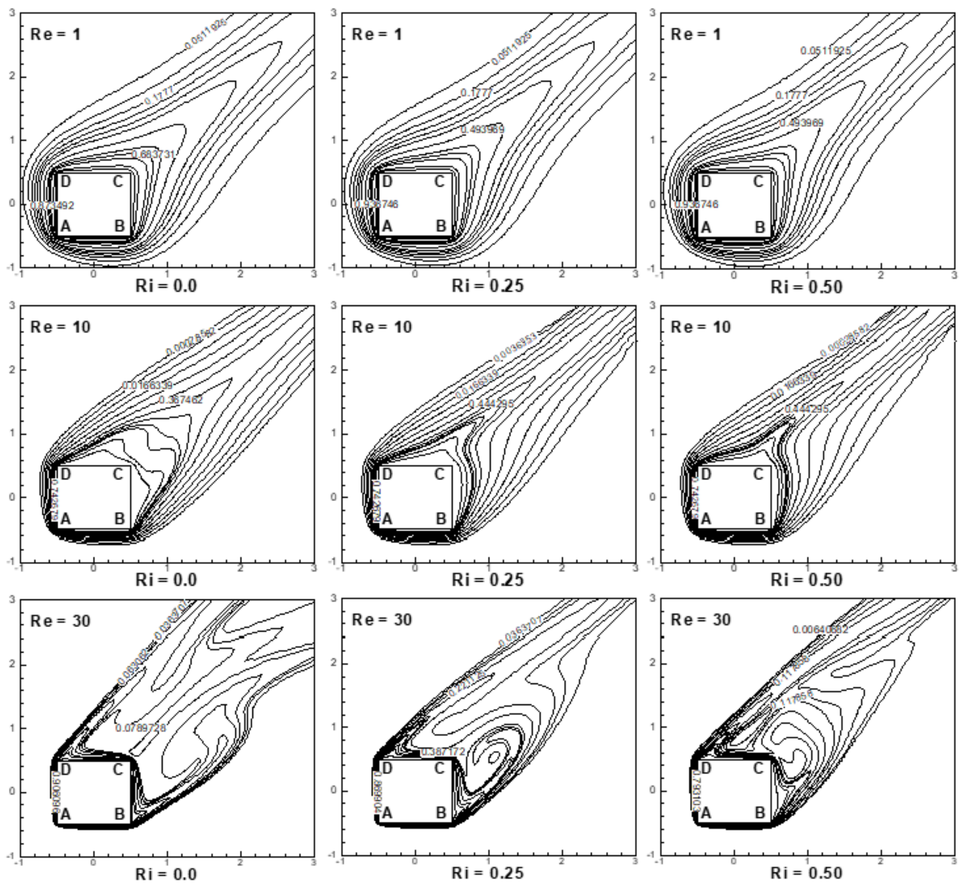

Figure 9. Isotherm patterns at Pr = 100, α = 45º, Re = 1, 10, 30 and Ri = 0.0, 0.25, 0.50.

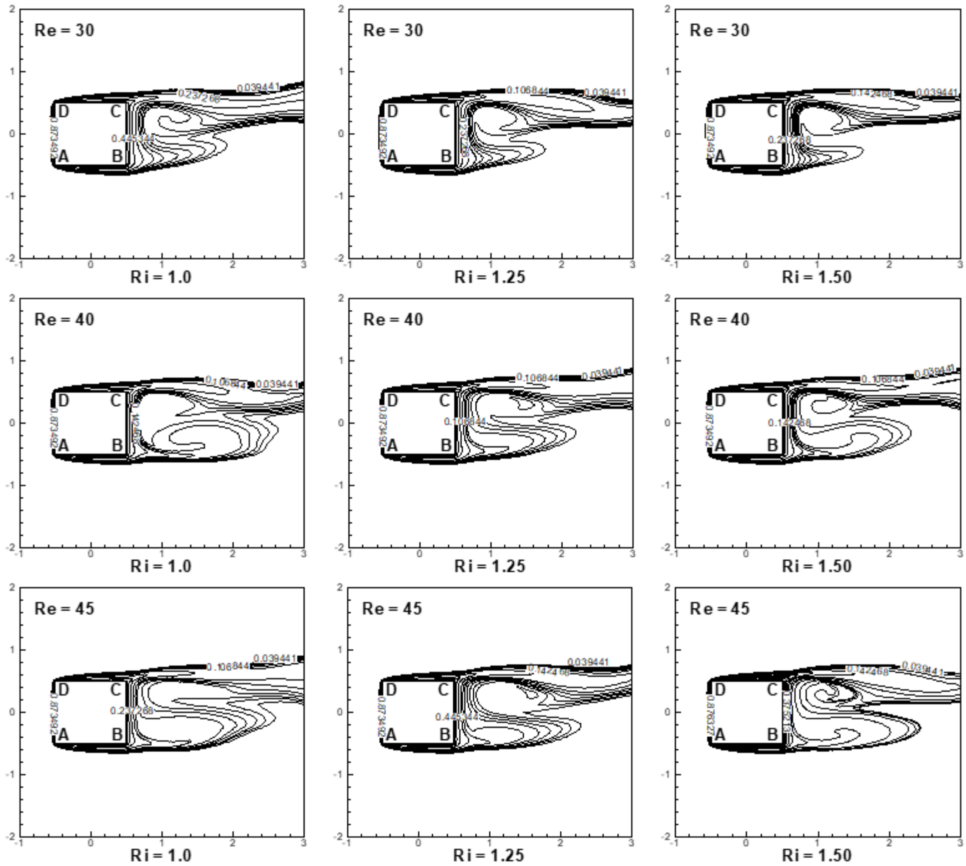

Figure 10. Isotherm patterns at Pr = 100, α = 90º, Re = 30, 40, 45 and Ri = 1.0, 1.25, 1.50.

The crowding of isotherms are observed more on leading face(s) of cylinder in comparison with other faces of cylinder as shown in Figs. 8-10 for condition ($0 \le Ri \le 1.50$, $1 \le Re \le 45, 0^o \le \alpha \le 90^o$, $\phi = 0^o$, Pr = 100). The trends are observed similar for the range of Richardson number chosen. Crowding of isotherms move near to the cylinder surface either with increase in Ri or Re as shown in Figs. 8-10. Similar trends have been observed for entire free-stream orientations range. More accumulation of isotherms on front face(s) of cylinder leading to higher rate of heat transfer from front face(s). The rate of heat transfer increases further either with increase in Richardson number or Reynolds number due to the fact that momentum of the fluid particles increases with the increase in Richardson or Reynolds numbers. More heated fluid particles replacement is observed from the colder fluid particles with increasing Richardson and Reynolds numbers leading to higher heat transfer rate from all the faces of square cylinder.

4.2. Surface Pressure and Surface Vorticity

Variation of surface pressure and surface vorticity at Re = 1 - 45, Ri = 0 - 1.50, $\alpha = 0^o$- 90^o, Pr = 100 and $\phi = 0^o$ is shown in Figs. 11-12. It is shown in Fig. 11 that the cylinder surface pressure is observed highest on the front face(s) (AB, AB and AD, AD at $\alpha = 0^o$, $\alpha = 45^o$ and $\alpha = 90^o$) of the cylinder that is placed in front of the free-stream. Surface pressure is noticed minimum on the rear face(s) (CD, CD and BC, BC at $\alpha = 0^o$, $\alpha = 45^o$ and $\alpha = 90^o$) of the cylinder and intermittent for the side faces of the cylinder. Similar trends are seen for the range of free-stream orientations chose. It is shown in figure that with increase in the magnitudes of Reynolds number the pressure on the front face(s) decreases to a minimum due to an increase in the momentum of fluid particles with an increase in the magnitudes of Reynolds number. Pressure increases on the rear face(s) as the Reynolds number increase. The trend for the whole range of free-stream orientations is observed similar. An increment in the magnitude of Richardson number, leading to an increases in pressure gradient in the stream wise direction across the square cylinder for the selected range of Reynolds number chosen. Similar trends have been observed for the chosen range of the orientations of free-stream. The pressure at the vertices (A, B, C and D) of the cylinder is found to be maximum for the chosen parametric range, and it decreases due to acceleration (inertia/buoyancy induced) of the fluid particles around the cylinder vertices.

It is seen from Fig. 12 at $1 \le Re \le 45$, $0 \le Ri \le 1.50$, $0^o \le \alpha \le 90^o$, $\phi = 0^o$ and Pr = 100 that the vorticity along the surface is observed large on leading face(s) of cylinder for entire range α. Surface vorticity changes its sign across the stagnation point that lies on leading face(s) of cylinder as shown in Fig. 12.

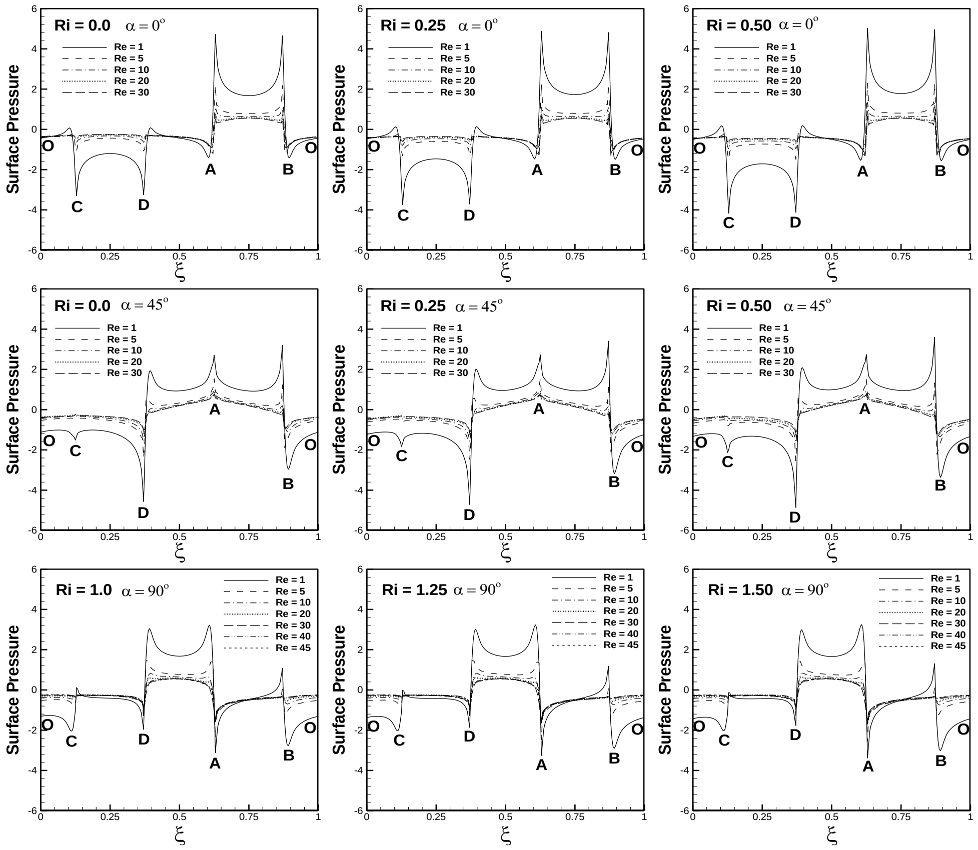

Figure 11. Variation of cylinder surface pressure $1 \le Re \le 45$, $0 \le Ri \le 1.50$, $\alpha = 0^o, 45^o, 90^o$.

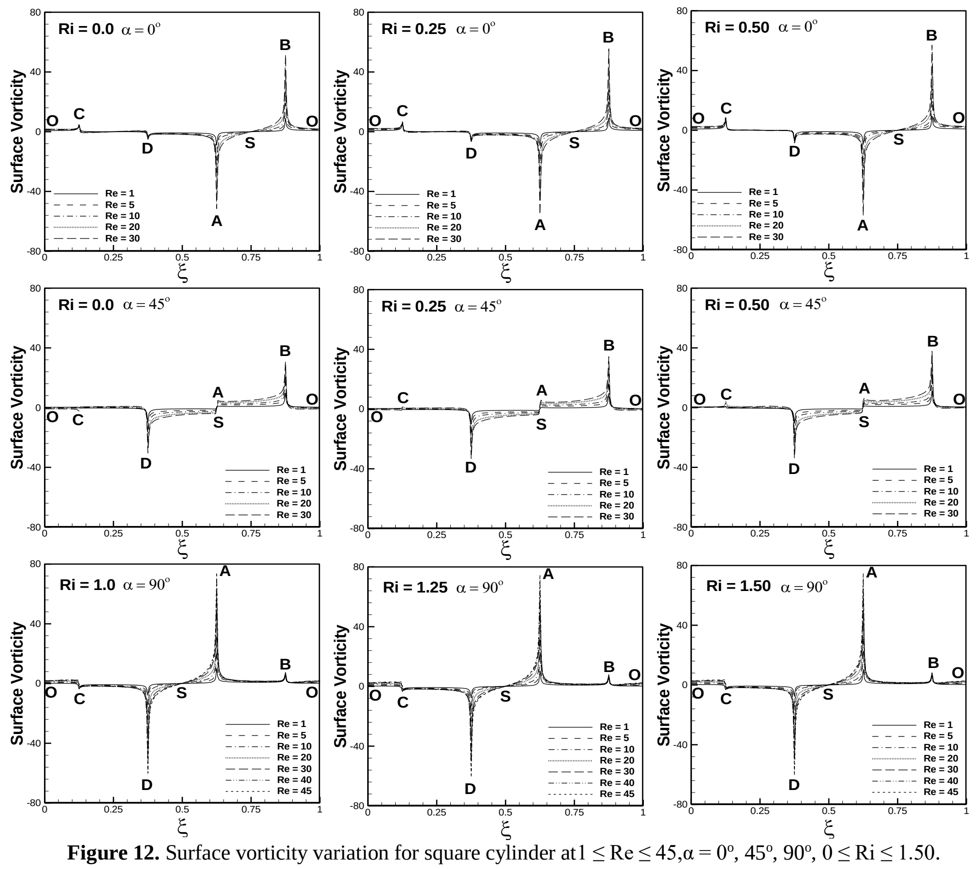

Figure 12. Surface vorticity variation for square cylinder at $1 \le Re \le 45$, $\alpha = 0^o, 45^o, 90^o$, $0 \le Ri \le 1.50$.

Magnitude of surface vorticity increases with increasing Reynolds number for the chosen range of orientations of the free-stream. Magnitude of surface vorticity also increases with increasing Ri, increase in Ri resulting in momentum gain of the shear layers which further increases the velocity of fluid particles and hence high surface vorticity. The vorticity is found to be maximum at the vertices adjacent to the front face(s) of the cylinder in comparison with other vortices. The reason is the large fluid particle velocities around the front face(s) vertices. This happens for the entire range of α.

4.3. Time Histories of Lift and Drag Coefficients

Figure 13 and figure 14 shows the variation of coefficients of lift and drag (C_L and C_D) with respect to non-dimensional time at $1 \leq Re \leq 45$, $0 \leq Ri \leq 1.50$, $0^o \leq \alpha \leq 90^o$, $\phi = 0^o$ and Pr = 100. It is depicted in time histories of lift& drag coefficients in figure 13 and figure 14 that the flow is found to be steady over the chosen range of free-stream orientations, Reynolds and Richardson numbers, except at Re = 30, $\alpha = 45^o$ and $20 \leq Re \leq 45$, $\alpha = 90^o$. At a Reynolds number Re = 30, $0 \leq Ri \leq 0.50$ and $\alpha = 45^o$ the onset of vortex-shedding is observed and the flow becomes unsteady and periodic flow. Figure 13 shows that the high amplitudes of lift coefficient for $\alpha = 45^o$ are observed due to the shedding of big size vortices on the downstream side of the cylinder wake. It can be seen from Fig. 13 that for $\alpha = 0^o$, the lift coefficient (negative) is found to be maximum at Re = 1 and decreases with increase in Reynolds number. Similar trends have been observed for the entire range of Richardson number. At $\alpha = 45^o$ and 90^o, positive lift coefficient is found to occur at Re = 1 and changes to negative lift coefficient at higher magnitudes of Reynolds number. The lift coefficient (negative) is found to be maximum for Re = 30 at $\alpha = 45^o$ and Re = 20 at $\alpha = 90^o$. The trend remains same for the entire range of Richardson number.

Figure 14 indicates that the drag coefficient decreases substantially over the whole range of Richardson number with an increase in the magnitudes of Reynolds number. The pattern for the whole range of free-stream orientations is observed same. Magnitudes of drag coefficient increase substantially with an increase in magnitudes of Richardson number at Re = 1, and observed least for other selected Reynolds number. The effects of Ri is dominating at small magnitudes of Re and least at large magnitudes of Re as depicted in Fig. 14.

4.4. Mean Lift Coefficient, Mean Drag Coefficient and Mean Coefficient of Moment

Mean (time mean) lift coefficient (C_L) variation with Ri is shown in Fig. 15 for $1 \leq Re \leq 45$, $0 \leq Ri \leq 1.50$, $\alpha = 0^o$, 45^o& 90^o, Pr = 100 and $\phi = 0^o$. It is shown in figure that the mean lift coefficient either negative or positive increases with increasing Richardson number. Similar trends are observed for the entire free-stream orientations range. With reference to Fig. 1 negative lift coefficient means C_L is in downward direction and towards right. It is depicted in Fig. 15 that the magnitude of mean coefficient of lift is observed maximum at Re = 20, Ri = 1.5 and $\alpha = 90^o$. For the chosen range of Re, mean lift coefficient variation is observed minimum (of the order of 10^{-3} i.e. nearly zero) with increasing Ri at $\alpha = 0^o$. For the entire Reynolds number range the mean lift coefficient variation with Richardson number is found to be large at $\alpha = 45°$ and 90^o. At $\alpha = 0^o$ and with an increase in Reynolds number for a fixed Richardson number, the mean lift coefficient is shifted towards zero. At $\alpha = 45^o$ and 90^o, the mean lifting coefficient for a given Richardson number is changed from + ve to –ve with an increasing Reynolds number other than Ri = 0 and $\alpha = 90^o$. The pressure gradient across the cylinder in transverse direction increases with increasing Re, resulting in high mean lift coefficient. Effect of Re on mean coefficient of lift is dominating as depicted in Fig. 15. Significant effects of Richardson number on mean lift coefficient is observed.

Figure 16 depicts the mean drag coefficient (C_D) variation with Ri at $1 \leq Re \leq 45$, $0 \leq Ri \leq 1.50$, $\alpha = 0^o$, 45^o& 90^o, Pr = 100 and $\phi = 0^o$. Figure 16 shows that the mean drag coefficient at a fixed magnitude of Richardson number decreases with an increase in the Reynolds number for the whole free-stream orientations range. For the chosen range of Richardson number, the mean coefficient of drag is always observed to be highest at Re = 1. The trend for the chosen range of free-stream orientations is observed similar. The pressure gradient across the cylinder in stream wise direction is found more at lower magnitudes of Reynolds number leading to large mean drag coefficient. Effects of Reynolds number are dominating and effects of Richardson number are slight on mean drag coefficient as depicted in Fig. 16.

Mean moment coefficient variation with Ri is shown in Fig. 17 for $1 \leq Re \leq 45$, $0 \leq Ri \leq 1.50$, $0^o \leq \alpha \leq 90^o$, Pr = 100 and $\phi = 0^o$. It is seen from figure that mean moment coefficient (C_M) variation with Ri and Reynolds number is slight (nearly zero, of the order of 10^{-3}) for$\alpha = 0^o$. For the chosen Re range, mean moment coefficient increases with increase in Ri at $\alpha = 45^o$ and 90^o. For the range of Ri chosen, the mean moment coefficient decreases with increase in Re except for Ri = 0, $\alpha = 45^o$ and 90^o as depicted in Fig. 17. At Ri = 0 the mean moment coefficient is found nearly zero for the entire range of Reynolds number. Mean moment coefficient for selected range of Richardson number is always observed highest at Re = 1. Same trend is observed for the chosen range of orientations of the free-stream.

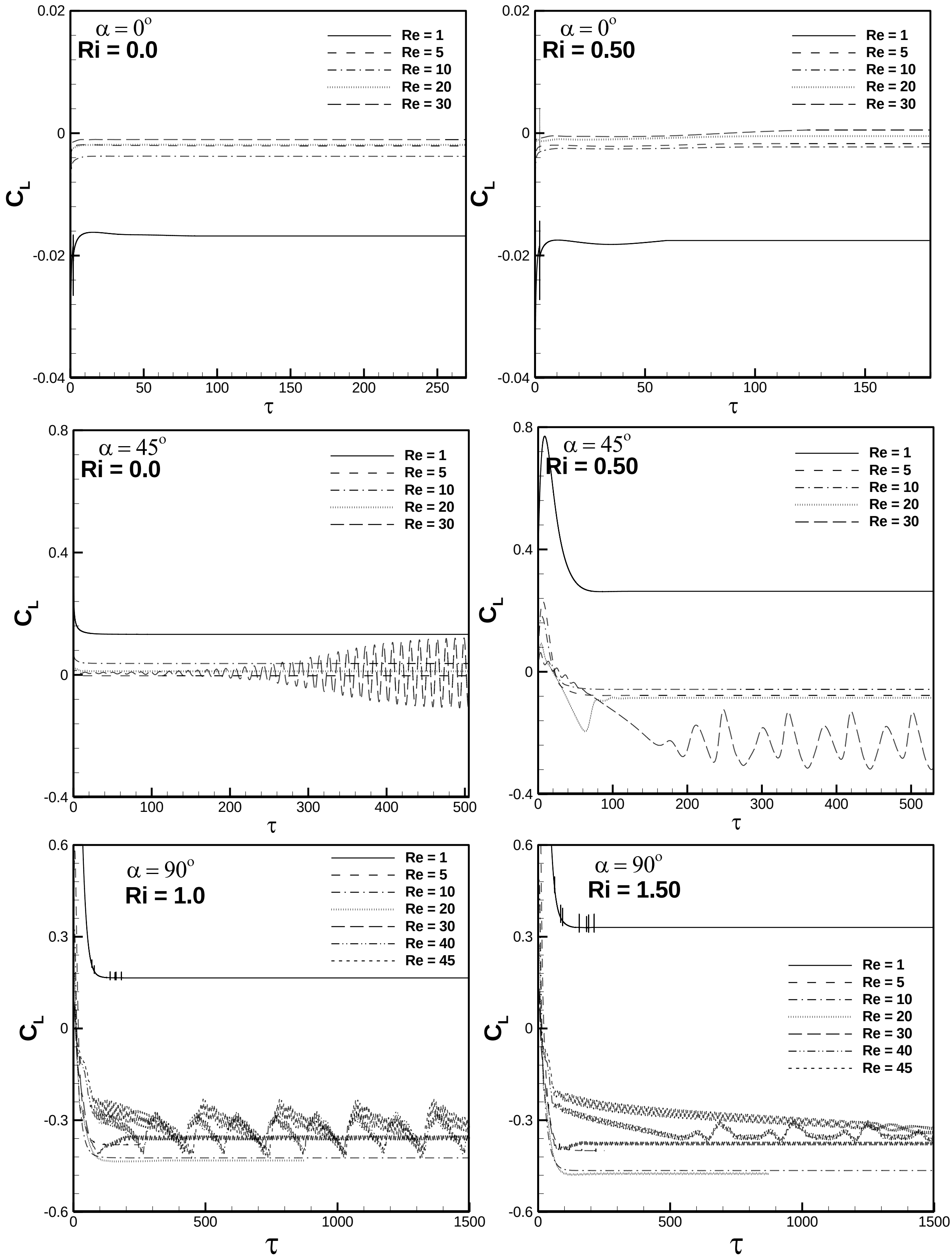

Figure 13. Variation of C_L with τfor $1 \leq Re \leq 45$, $0 \leq Ri \leq 1.50$, α = 0°, 45°& 90° at Pr = 100, ϕ = 0°.

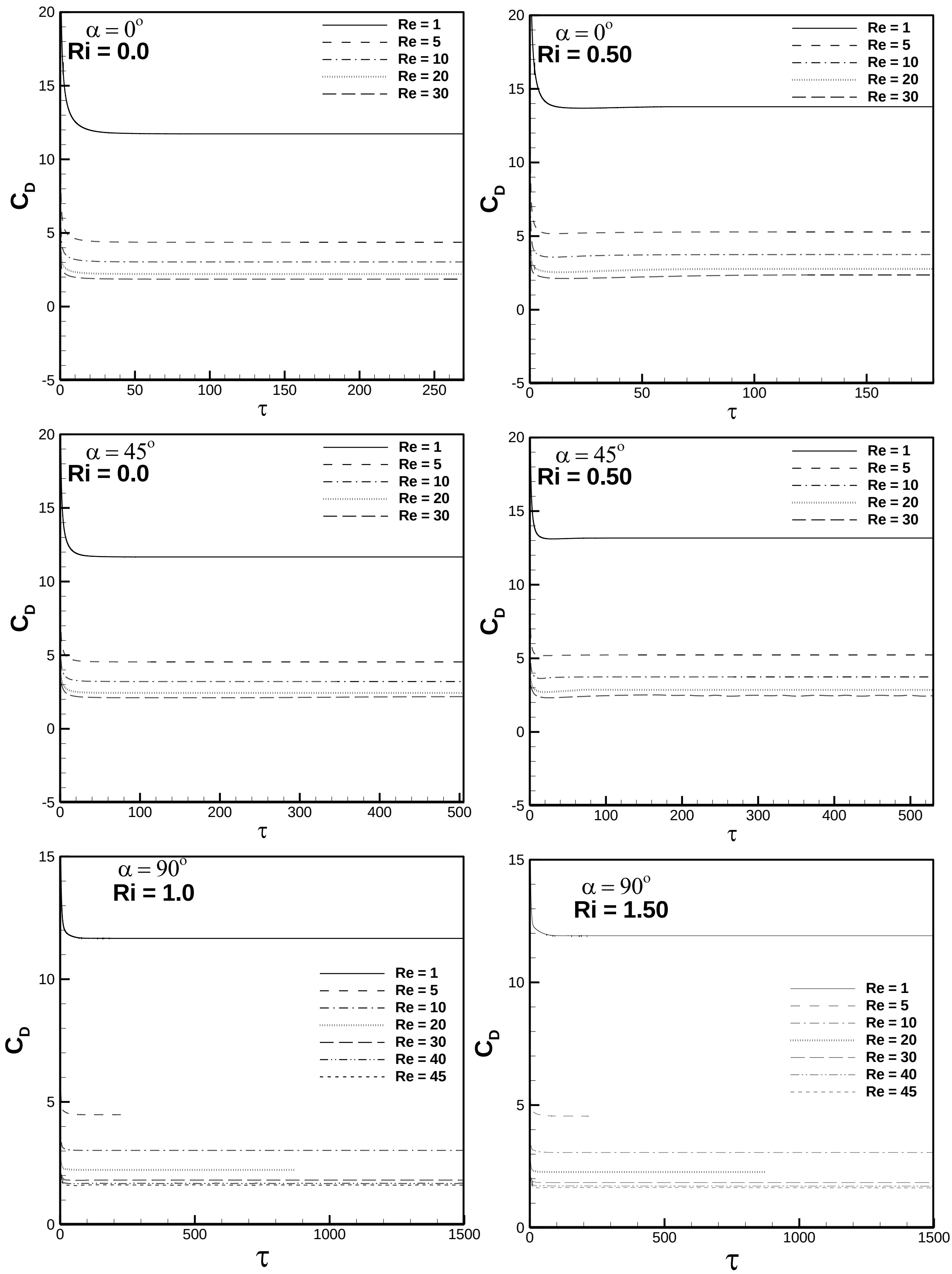

Figure 14. Variation of C_D with $\tau$for $1 \leq Re \leq 45$, $0 \leq Ri \leq 1.50$, $\alpha = 0^o, 45^o\& 90^o$ at $Pr = 100$, $\phi = 0^o$.

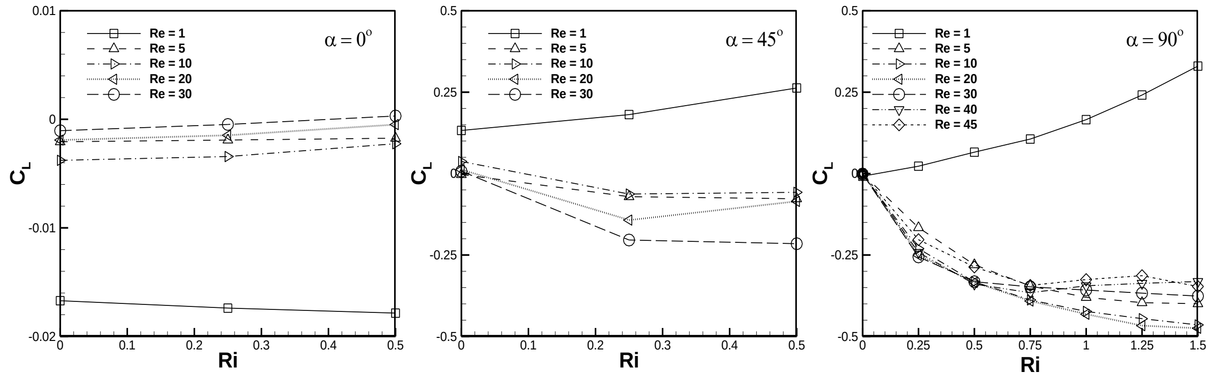

Figure 15. Variation of mean C_L with Richardson number for $1 \leq Re \leq 45$, $\alpha = 0^o$, 45^o& 90^o at Pr = 100.

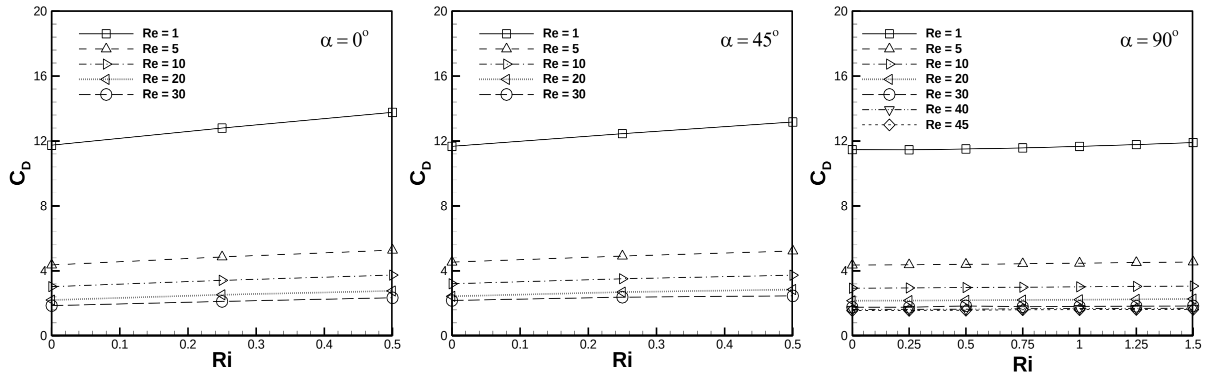

Figure 16. Variation of Mean C_D with Ri at $1 \leq Re \leq 45$, $0 \leq Ri \leq 1.50$, $\alpha = 0^o, 45^o, 90^o$ at Pr = 100.

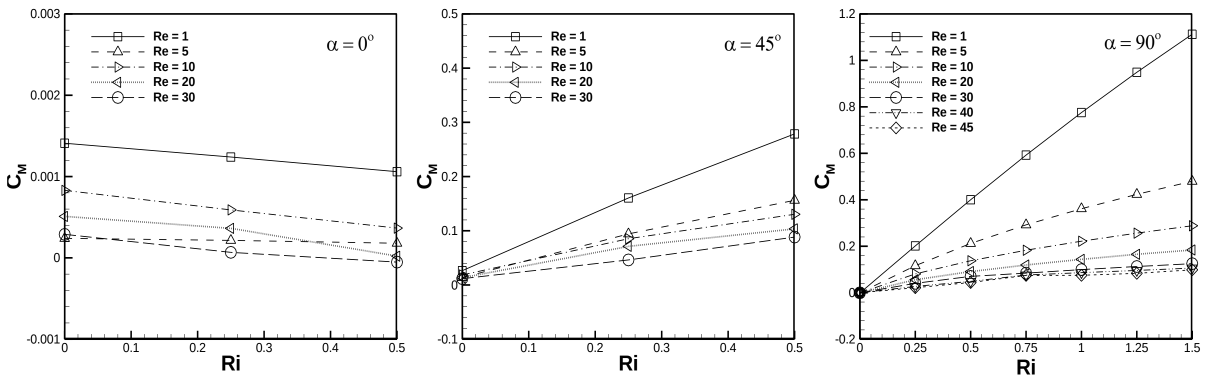

Figure 17. Variation of Mean moment Coefficient (C_M) with Ri for $1 \leq Re \leq 45$, $0 \leq Ri \leq 1.50$, $\alpha = 0^o, 45^o, 90^o$ at Pr = 100.

4.5. Surface Nusselt Number (Nu_L) and Mean Nusselt Number (Nu)

Figure 18 shows the local Nusselt number (Nu_L) variation around the square cylinder surface at $1 \leq Re \leq 45$, $0 \leq Ri \leq 1.50$, $0^o \leq \alpha \leq 90^o$, $\phi = 0^o$ and Pr = 100. It is seen from Fig. 18 that the local Nusselt number is observed maximum from the leading side(s) of the cylinder, low from the trailing side(s) of the cylinder and intermittent from the remaining side(s) of the square cylinder for the chosen range of orientations of the free-stream. With the rise in the magnitudes of Reynolds number and Richardson number, heat transfer from all sides of the cylinder increases. As can be seen from the figure 18 that the influence of Reynolds number on heat transfer is dominating.

The heat transfer rate from the square cylinder vertices is found to be maximum as shown in Figure 18. Increase in the magnitudes of Reynolds or Richardson numbers increases the fluid particles momentum, replaces the heated fluid particles at a faster rate from the faces and vertices of the cylinder with the relatively colder particles of the fluid, improves the heat transfer rate from the cylinder.

Time mean (mean) Nusselt number (Nu) variation with Ri is depicted in figure 19 for the conditions (Re = 1 -45, Ri = 0 - 1.50, $\alpha = 0^o - 90^o$, Pr = 100, $\phi = 0^o$). It is depicted in Fig. 19 that the variation in mean Nusselt number with Richardson number is minimum for the whole range of Re. The trend for the selected range of free-stream orientations is observed the same. At a fixed magnitude of the Ri, the Nusselt number significantly increases with an increase in the magnitudes of Re for the range of free-stream orientations chosen. The rise in the magnitudes of Reynolds number increases the velocity of fluid particles, resulting in quick displacement of warmer fluid particles in the vicinity of square cylinder from the cooler fluid particles of the approaching free-stream. The rate of heat transfer from the cylinder increases with the increase in Reynolds number and Richardson number.

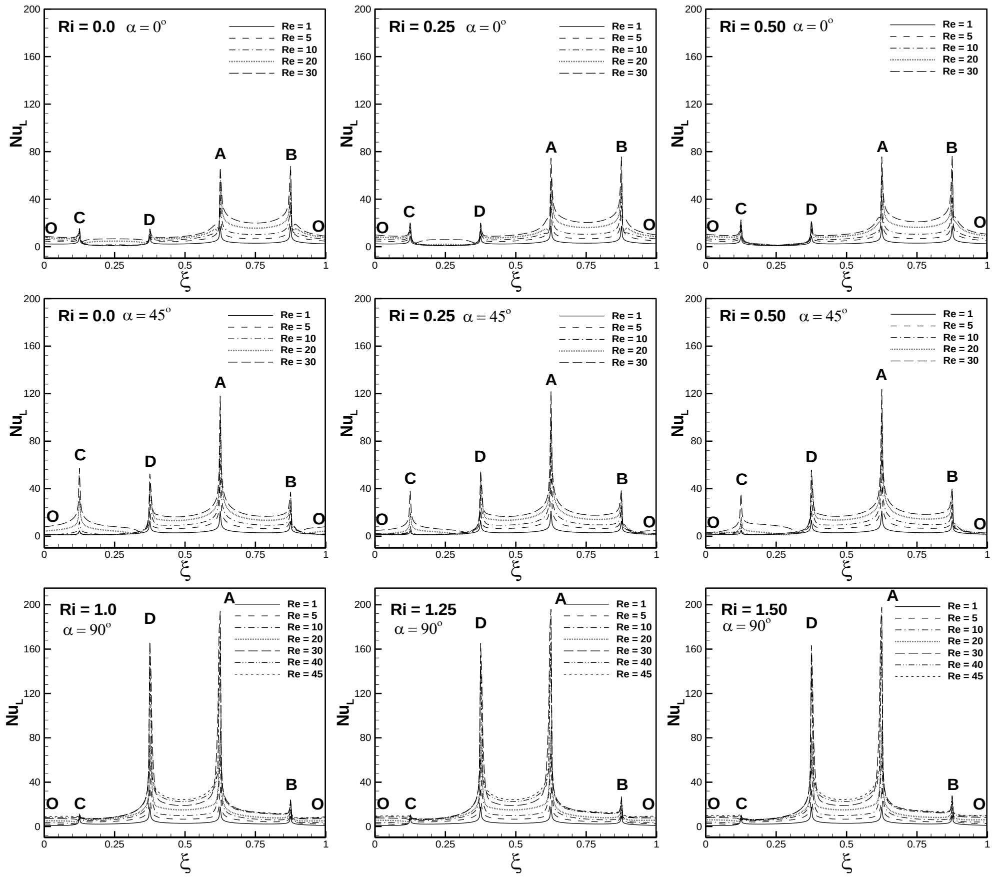

Figure 18. Local Nusselt number variation for 1 ≤ Re ≤ 45, 0 ≤ Ri ≤ 1.50 and α = 0º, 45º, 90º.

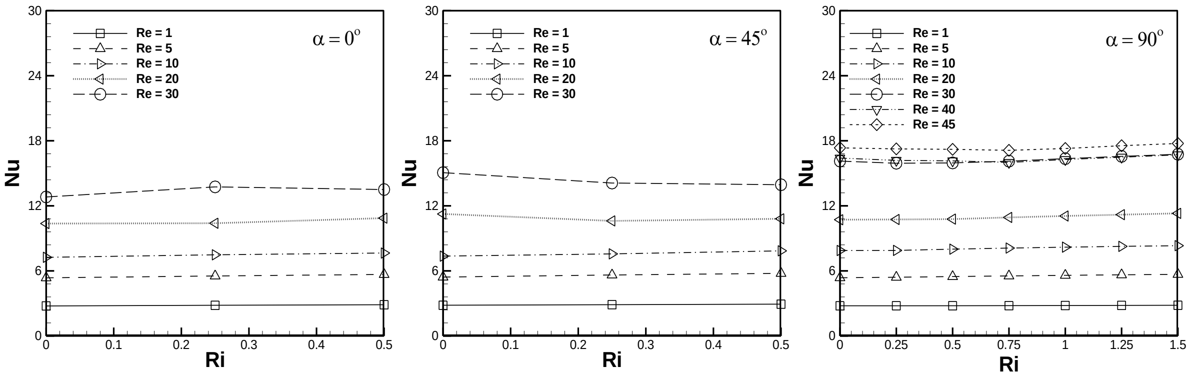

Figure 19. Variation of mean Nu with Ri for 1 ≤ Re ≤ 45, 0 ≤ Ri ≤ 1.50, α = 0º, 45º, 90º at Pr = 100, ϕ = 0º.

5. CONCLUSIONS

In the current study the effects of Richardson number and Reynolds number with free-stream orientations on fluid dynamics and heat transfer characteristics are examined in detail for $1 \leq Re \leq 45$, $0 \leq Ri \leq 1.50$, $0^o \leq \alpha \leq 90^o$ and $Pr = 100$ at a fixed cylinder orientation $\phi = 0^o$. The following conclusions have been made;

1. The flow is found to be steady for $1 \leq Re \leq 30$, $0 \leq Ri \leq 0.50$ at $\alpha = 0^o$, $1 \leq Re \leq 20$, $0 \leq Ri \leq 0.50$ at $\alpha = 45^o$, and $1 \leq Re \leq 10$, $1.0 \leq Ri \leq 1.50$ at $\alpha = 90^o$, respectively. Vortex-shedding initiation or onset is observed at Re = 30, $0 \leq Ri \leq 0.50$ and $\alpha = 45^o$, the flow becomes unsteady and periodic flow. No vortex is observed at Re = 1, the vortices are induced at higher magnitudes of Reynolds number. The vortices are increased in size with increasing Reynolds number, and reduces in size with the increase in Richardson number.
2. Surface pressure and surface vorticity are found to be maximum on leading face(s) of cylinder that faces the upcoming stream of the fluid. Surface pressure is observed to be minimum on the trailing face(s) and intermittent on the side faces of the cylinder. It is identified that the surface vorticity changes its sign (+ve or -ve) across the stagnation point that is generated on the cylinder leading face(s). The surface pressure and surface vorticity is seen maximum at corners of square cylinder.
3. It is found that mean coefficient of lift (C_L) increases with increasing Ri for the selected range of free-stream orientations. Variation of mean lift coefficient is of the order of 10^{-3} that is nearly zero with increasing Richardson number for$\alpha = 0^o$. For the chosen range of Re, variation of mean coefficient of lift with Ri is found large at $\alpha = 45^o$and 90^o.Magnitude of mean drag coefficient (C_D) reduces significantly for the whole range of free-stream orientations with an increase in Reynolds number. The mean drag coefficient for the range of Richardson number is always observed highest at Re = 1.Moment coefficient (time mean) variation with Ri and Re is slight (nearly zero, of the order of 10^{-3}) at $\alpha = 0^o$. Magnitude of moment coefficient rises as the magnitude of Ri is increased at $\alpha = 45^o$ and 90^o for the chosen Reynolds number range. The mean moment coefficient for the range of Richardson number selected is always observed highest at Re = 1.
4. The crowding of isotherms are observed maximum on the leading face(s) of the cylinder in comparison with other faces of cylinder. Crowding of isotherms on the leading face(s) of cylinder further increases with increasingRichardson numberor Reynolds number, resulting in more heat transfer from the leading face(s) of the cylinder.
5. It is observed that the local heat transfer (Nu_L) increases with the increase in Reynolds number or Richardson number. Heat transfer from the vertices of cylinder is found maximum and increases further with increase in Reynolds/Richardson numbers owing to the rapid exchange of warm fluid particles with cooler fluid particles. Mean Nusselt number (Nu) at a fixed magnitude of Ri increases with increasing Re for the selected range of orientations of the free-stream. It is observed that the rate of heat transfer increases either with increase in Richardson number or Reynolds number or both.

REFERENCES

[1] Sohankar A., Norberg C. and Davidson L., “Low-Reynolds number flow around a cylinder at incidence: study of blockage, onset of vortex shedding and outlet boundary condition”, *Int. J. Nume. Meth. Fluids* 26, pp. 39 – 56, 1998.

[2] Sharma A. and Eswaran V., “Effect of aiding and opposing buoyancy on the heat and fluid flow across a square cylinder at Re = 100”, *Nume. Heat Trans. Part A* 45, pp. 601 – 624, 2004.

[3] Sharma A. and Eswaran V., “Effect of channel-confinement and aiding/opposing buoyancy on the two-dimensional laminar flow and heat transfer across a square cylinder. *Int. J. Heat and Mass Trans.* 48, pp. 5310 – 5322, 2005.

[4] Chatterjee D. and Mondal B., “Effect of thermal buoyancy on the two-dimensional upward flow and heat transfer around a square cylinder”, *HeatTrans. Engg.* 33 (12), pp. 1063 – 1074, 2012.

[5] Dhiman A., Sharma N. and Kumar S., “Buoyancy-aided momentum and heat transfer in a vertical channel with a built-in square cylinder”, *Int. J. Sust.Energy* 10.1080/14786451.2013.764878, pp. 1 – 22, 2013.

[6] Yang G. and Wu J., “Effect of side ratio and aiding/opposing buoyancy on the aerodynamic and heat transfer characteristics around a rectangular cylinder at low Reynolds numbers”, *Nume. Heat Trans. Part A* 64, pp. 1016 – 1037, 2013.

[7] Moulai S., Korichi A. and Polidori G., “Aided mixed convection past a heated square cylinder”, *Journal of Applied Fluid Mechanics*, Vol. 9, No. 1, pp. 303 – 310, 2016.

[8] Rashid A. and Hasan N.,“Vortex-shedding suppression in mixed convective flow past a heated square cylinder”, Int. J. Mech. Mecha. Engg. 5, 6, pp. 953-961, 2011.

[9] Rashid A. and Hasan N.,“Influence of free-stream orientation and buoyancy on aerodynamic characteristics in mixed convective flow past a square cylinder”, Proc. 5th Int. Conf. Adv. Mech. Engg. (ICAME-2011), pp. 329-334, 2011.

[10] Rashid A. and Hasan N., “Effect of free-stream orientation and buoyancy on heat transfer in mixed convective flow past a square cylinder”, World Academy of Science, Engg. Tech. 79 pp. 471-478, 2011.

[11] Haider S. A. and Rashid A., “Mixed convective flow past a square cylinder with variable Prandtl number”, Nat. Conf. Mech. Engg. Ideas, Innovations and Initiatives (NCMEI3-2016), pp. 339-344, 2016.

[12] AnshumaanS. and Rashid A.,“Effect of Buoyancy and Inertia Forces on the Flow Past a Heated Square Cylinder in Cross Flow Configuration”, Adv. Sci. Engg. Med., 10, 3, pp. 505-512, 2018.

[13] Rashid A. and Hasan N.,“Steady and Unsteady Flow Regimes in Two-Dimensional Mixed Convective Flow of Air past a Heated Square Cylinder” Int. J. Mech. Sci. Vol. 175, 105533, 2020.

[14] Yuan Ma., Mohebbi R., Rashidi M. M. and Yang Z., “Numerical simulation of flow over a square cylinder with upstream and downstream circular bar using lattice Boltzmann method” Int. J. Mod. Phy. C, 29, 4, 1850030, 2018.

[15] Yuan Ma., Rashidi M. M. and Yang Z., “Numerical simulation of flow past a square cylinder with a circular bar upstream and a splitter plate downstream”, J. Hydro., 31(5), 949-964,2019.

[16] Rafik B., Yacine K. and Faouzi S., “Unconfined laminar nanofluid flow and heat transfer around a square cylinder

with an angle of incidence", Jordan Journal of Mechanical and Industrial Engineering, 13, 191-196, 2019.

[17] Tritton D. J., "*Physical fluid dynamics",* ELBS Edi. Chap. 13, pp. 127 – 130, 1979.

[18] Thompson J. F., Warsi Z. U. A. and Mastin C. W.,"*Numerical grid generation foundations and applications".* North Holland, 1985.

[19] Hasan N., Anwer S. F. and Sanghi S., "On the outflow boundary condition for external incompressible flows: A new approach", *J. Compu. phys.* 206, pp. 661 – 683, 2005.

[20] Cheng L. and Armfield S."A simplified marker and cell method for unsteady flows on non-staggered grids". Int. J. Nume. Meth. Fluids 21 (1), 15 – 34, 1995.

[21] Gresho P. M.,"Incompressible fluid dynamics: some fundamental formulation issue". Annu. Rev. Fluid Mech. 23, 413 – 454, 1991.

[22] Hasan N. and Rashid A., "Vortex-shedding suppression in two-dimensional mixed convective flows past circular and square cylinders", *Phys. Fluids* 25 (053603), pp. 1 – 27, 2013.

[23] Hasan N. and Sanghi S., "The dynamics of two-dimensional buoyancy driven convection in a horizontal rotating cylinder", *J. Heat Trans.* 126, pp. 963 – 984, 2004.

[24] Kuwahara K., "Unsteady flow simulation and its visualization", 30th AIAA *Fluid Dyna. Conf.* AIAA, 99 – 3405, 1999.

[25] Rhie C. M. and Chow W. L., "Numerical study of the turbulent flow past an airfoil with trailing edge separation", *AIAA J*. 21 (11), pp. 1525 – 1532, 1983.

[26] Dhiman A. K., Chhabra R. P., Sharma A. and Eswaran V., "Effects of Reynolds and Prandtl numbers on heat transfer across a square cylinder in the steady flow regime", *Nume. Heat Trans. Part A* 49, pp. 717 – 731, 2006.

[27] Paliwal B., Sharma A., Chhabra R. P. and Eswaran V., "Power law fluid flow past a square cylinder: Momentum and heat transfer characteristics", *Chem. Eng. Sci.* 58, pp. 5315 – 5329, 2003.

[28] Dhiman A. K., Anjaiah N., Chhabra R. P. and Eswaran V., "Mixed convection from a heated square cylinder to Newtonian and Power-law fluids", *J. Fluids Eng.* 129 (4), pp. 506 – 573, 2006.

[29] Rashid A., "A numerical investigation of two-dimensional mixed convective flow past a square cylinder", *Doctoral thesis*, http://ir.amu.ac.in/id/eprint/9861, 2016.

[30] Rashid A., "A numerical investigation of two-dimensional mixed convective flow past a square cylinder", *Doctoral thesis*, https://shodhganga.inflibnet.ac.in/handle/10603/117546, 2016.

[31] Rashid A., Shahrukh V. Mubashshir A. A. and Anwar S. F., "Numerical investigation of fluid flow past a square cylinder in mixed convective flow regime", IOP Conference Materials Science and Engineering, doi:10.1088/1757-899X/691/1/012038, 2019.

[32] Okajima A., "Strouhal numbers of rectangular cylinders". J. Fluid Mech. 123, 379-398, 1998.

[33] Luo S. C., Chew Y. T. and Ng Y. T., "Characteristics of square cylinder wake transition flows". Phys. Fluids 15 (9), 2549 – 2559, 2003.

[34] Collis D. C. and Williams M. J.., "Two-dimensional convection from heated wires at low Reynolds numbers". J. Fluid Mech. 06:357-84, 1959.

[35] Wang A.-B. and Travnicek Z., "On the linear heat transfer correlation of a heated circular cylinder in laminar cross flow using a new representative temperature concept". Int. J. Heat and Mass Transfer 44:4635, 2001.

[36] Wang A.-B., Travnicek Z. and Chia K.-C., "On the relationship of effective Reynolds number and Strouhal number for the laminar vortex shedding of a heated circular cylinder". Phys. Fluids 12, 6 1401, 2001.

[37] Saha A. K., Muralidhar K. and Biswas G., "Transition and chaos in two-dimensional flow past a square cylinder". J. Engg. Mech. 125, 523 – 532, 2000.

[38] Ranjan R., Dalal A. and Biswas G., "A numerical study of fluid flow and heat transfer around a square cylinder at incidence using unstructured grids". Nume. Heat Trans. Part A 54, 890 – 913, 2008.

[39] Yoon D-H., Yang K-S. and Choi C-B.,"Flow past a square cylinder with an angle of incidence". Phys. Fluids 22 (043603), 1 – 12, 2010.